INVESTIGATION OF ANHARMONIC EFFECTS IN PHONON TRANSPORT

A Thesis Submitted to
the Graduate School of Engineering and Sciences of
İzmir Institute of Technology
in Partial Fulfillment of the Requirements for the Degree of

MASTER OF SCIENCE

in Materials Science and Engineering

by
Mustafa Neşet Çınar

July 2018
İZMİR

We approve the thesis of **Mustafa Neşet Çınar**

Examining Committee Members:

Assoc. Prof. Dr. Hâldun SEVİNÇLİ
Department of Materials Science and Engineering, İzmir Institute of Technology

---

Assoc. Prof. Dr. ÖZGÜR ÇAKIR
Department of Physics, İzmir Institute of Technology

Assoc. Prof. Dr. Alev Devrim GÜÇLÜ
Department of Physics, İzmir Institute of Technology

Assoc. Prof. Dr. Umut ADEM
Department of Materials Science and Engineering, İzmir Institute of Technology

---

Assoc. Prof. Dr. Gürsoy Bozkurt AKGÜÇ
Department of Physics, İzmir University of Economics

06 July 2018

Assoc. Prof. Dr. Hâldun SEVİNÇLİ
Supervisor, Materials Science and Engineering
İzmir Institute of Technology

Assoc. Prof. Dr. ÖZGÜR ÇAKIR
Co-Supervisor, Department of Physics
İzmir Institute of Technology

Prof. Dr. Mustafa M. DEMİR
Head of the Department of
Materials Science and Engineering

Prof. Dr. Aysun SOFUOĞLU
Dean of the Graduate School of
Engineering and Sciences

ACKNOWLEDGMENTS

I would like to thank my thesis supervisor Assoc. Prof. Dr. Hâldun SEVİNÇLİ for his patient guidance and encouragement throughout this study. I have learned much about computational science during my graduate education in Materials Science and Engineering Department in IZTECH and I am very grateful to him.

I would also like to express my gratitude towards my thesis co-supervisor Assoc. Prof. Dr. Özgür ÇAKIR for introducing complex physics concepts in a simpler way, making undergraduate lectures fruitful for me as a former undergraduate student of Physics Department at IZTECH.

I would like to thank the thesis commitee members Assoc. Prof. Dr. Gürsoy Bozkurt AKGÜÇ, Assoc. Prof. Dr. Alev Devrim GÜÇLÜ and Assoc. Prof. Dr. Umut ADEM for their comments and suggestions on this study.

This work is supported by TÜBİTAK-ARDEB Scientific and Technological Research Project Program (1001) (Project No: #115F445).

I am also very grateful to my best friends İsmail ULUS and Rıza USLU for their emotional support and encouragement. They have been always there for me during good times and bad times. We had fun together and the time I have spent with them is priceless.

Finally, I would like to thank my parents Aytül and Necati ÇINAR, and my sister Yağmur ÇINAR for providing me endless love and caring throughout my life. They have always been by my side during hard times and their encouragement kept me motivated during my education.

ABSTRACT

INVESTIGATION OF ANHARMONIC EFFECTS IN PHONON TRANSPORT

Phonons are quantum mechanical particles corresponding to ionic vibrations. They are similar to electrons in a way that they interact with other particles and defects, and they are responsible for thermal conduction in insulators like electrons are responsible for electrical conduction in conductors. Most of the physical properties due to ionic vibrations can be determined by using harmonic approximation which consider phonons as independent quantum mechanical harmonic oscillators having quadratic potentials depending on the displacements of atoms in their equilbirium positions. However, there are some physical processes such as finite thermal conductivity and thermal expansion which cannot be explained with only harmonic phonons. To investigate these physical processes anharmonicity needs to be taken into account. Anharmonicity is related to the higher order terms in the interatomic potential and corresponds to phonon-phonon interactions. The strength of these interactions depends on the temperature which is related to the available thermal energy, or, the number of phonons given by the Bose-Einstein distribution. In this thesis, the effects of anharmonicity on quantum thermal transport are studied in nanoscale systems by using Green functions. Non-Equilibrium Green Functions (NEGF) method is a perturbative approach to study transport properties of both electronic and phononic systems. Anharmonic terms in interatomic potential are incorporated into NEGF method in the form of a self-energy which can be computed self-consistently. This approach provides high accuracy with high computational cost. As an alternative, mean field technique is computationally more feasible which allows to do calculations for larger systems. In this study, we investigate anharmonic transport properties of one-dimensional chains using NEGF method. Our calculations involve self-energies of third and fourth order anharmonic terms. In addition, mean field calculation for fourth order anharmonicity is performed for comparison.

ÖZET

FONON İLETİMİNDE ANHARMONİK ETKİLERİN İNCELENMESİ

Fononlar iyonik titreşimlere karşılık gelen kuantum mekaniksel parçacıklardır. Fononlar diğer paraçıklar ve kusurlarla etkileşme ve elektronların iletkenlerdeki elektriksel iletimden sorumlu olduğu gibi yalıtkanların ısıl iletimden sorumlu olma yönünden elektronlara benzemektedirler. İyonik titreşimlere bağlı olan fiziksel özelliklerin birçoğu, fononları atomların denge noktaları etrafında yer değiştirmelerine bağlı olan karesel potansiyele sahip bağımsız kuantum mekaniksel harmonik osilatörler olarak dikkate alan harmonik yaklaşma kullanılarak elde edilebilir. Fakat, sonlu ısıl iletkenlik ve ısıl genleşme gibi sadece harmonik fononlar ile açıklanamayan bazı fiziksel süreçler mevcuttur. Bu fiziksel süreçleri incelemek için anharmonisitenin dikkate alınması gerekir. Anharmonisite, interatomik potansiyeldeki yüksek dereceli terimlerle ilgilidir ve fonon-fonon etkileşimine karşılık gelmektedir. Bu etkileşimlerin gücü mevcut ısıl enerji veya Bose-Einstein dağılımıyla verilen, mevcut fonon sayısıyla ilgili olan sıcaklığa bağlıdır. Bu tezde anharmonisitenin ısıl taşınım üzerindeki etkileri nano ölçekteki sistemlerde Green fonksiyonları kullanılarak çalışılmıştır. Denge Dışı Green Fonksiyonları (NEGF) Yöntemi, hem elektronik hem de fononik sistemlerin taşınım özelliklerini çalışmak için olan bir pertürbatif yaklaşımdır. İnteratomik potansiyeldeki anharmonik terimler özuyumlu olarak hesaplanabilen bir özenerji biçiminde NEGF yöntemine dahil edilebilirler. Bu yaklaşım yüksek hesaplama maliyeti ile yüksek doğruluk sağlar. Alternatif olarak, ortalama alan tekniği, daha büyük sistemler için hesaplar yapmamızı sağlayan, hesaplama açısından daha olası bir yöntemdir. Bu çalışmada, NEGF yöntemini kullanarak tek boyutlu zincirlerin anharmonik taşınım özelliklerini araştırmaktayız. Hesaplarımız üçüncü ve dördüncü derece anharmonik terimlerin özenerjilerini içerir. Ek olarak, karşılaştırma için dördüncü derece anharmonisite için ortalama alan hesabı yapılmaktadır.

TABLE OF CONTENTS

LIST OF FIGURES

Figure **Page**

LIST OF SYMBOLS

δ . . . . . Kronecker Delta
h . . . . . Planck's constant
$\hbar$ . . . . . Reduced Planck's constant
k_{B} . . . . . Boltzmann Constant
e . . . . . Charge of an electron
m . . . . . Mass
t . . . . . Time
$\mathcal{G}$ . . . . . Electrical conductance
σ . . . . . Electrical conductivity
κ . . . . . Thermal conductance
κ_{el} . . . . . Electrical thermal conductivity
κ_{th} . . . . . Thermal conductivity
τ . . . . . Contour time
K . . . . . Harmonic force constant
K_n . . . . . n^{th} order force constant
ω . . . . . Frequency
G . . . . . Green function
g . . . . . Green function of uncoupled system
Σ . . . . . Self-energy
$\hat{a}$ . . . . . Annihilation operator
$\hat{a}^{\dagger}$ . . . . . Creation operator

LIST OF ABBREVIATIONS

DOS . . . . . Density of states
MFP . . . . . Mean free path
DFT . . . . . Density Functional Theory
QSCMF . . . . . Quantum Self-Consistent Mean-Field
NEGF . . . . . non-Equilibrium Green Function
SGF . . . . . Surface Green Function

CHAPTER 1

INTRODUCTION

1.1. Temperature and Heat

In classical statistical mechanics, equipartition theorem (Fowler (1967)) provides us a relation between mean energy and temperature. Energy of a system involves different degrees of freedom such as translational, vibrational and rotational. Heat can be transferred via energy exchange between different particles and different degrees of freedom.

As an example, suppose that there is some gas in a container, increasing the temperature of a small portion of the container will increase the kinetic energy of the particles in that portion. The kinetic energy as a form of heat will then be exchanged between each particle until the system reaches equilibrium, where all particles have the same average kinetic energy, that is, the same temperature.

There are three types of heat transfer, conduction, convection and radiation (Simon R. Phillpot (2005)). In solids, heat transport occurs by conduction. Conductivity is the measure of the ability to transfer heat under a temperature gradient. In metals, heat is transferred by a large number of free electrons as heat carriers. Thermal conductivity corresponding to this type of heat transer is called electrical thermal conductivity and Wiedemann-Franz Law describes the proportionality of electrical thermal conductivity to the electrical conductivity with a factor that depends on temperature, given by (Ziman (1972)),

$$\kappa_{\mathrm{el}} = \frac{\pi^2}{3}\frac{k_{\mathrm{B}}^2}{e^2}T\sigma \tag{1.1}$$

where κ_{el} is the electrical thermal conductivity, σ is the electrical conductivity, k_{B} is the Boltzmann constant, e is the charge of an electron (-1.602×10^{-19} C) and T is the temperature. Heat conduction is dominated by lattice conduction in semiconductors and insulators which have a small number or no free electrons available as heat carriers (Ziman (1972)).

In lattice conduction, heat is carried by vibrations of atoms with respect to their equilibrium positions (lattice points) along the system.By using harmonic approximation these vibrations can be modelled by classical waves. Although this approach leads to a

correct dispersion relation and density of states (Chen (2000)), to explain certain properties such as heat capacity these vibrations can be modelled as a superposition of quantum mechanical particles called phonons (Hofmann (2015)).

1.2. Lattice Vibrations and Phonons

In this section, the basic mathematical formulation for phonons is described. The first of the three subsections describes lattice vibrations as simple harmonic oscillators by using classical mechanics. The second one, then provide a description for harmonic oscillators using operator formalism via quantum mechanics. The third one describes phonons in many-body physics perspective.

1.2.1. Classical Model

The available thermal energy $k_{\mathrm{B}}\mathrm{T}$ at a definite temperature T where k_{B} is the Boltzmann constant, causes atoms to vibrate around their equilibrium positions at a certain frequency. Lattice potential causes the atoms to move around their equilibrium positions. These vibrations behave like waves with certain wavelengths corresponding to their frequencies. Depending on the orientation of the wave, there are different polarizations such as transverse and longitudinal. A visualization of transverse vibrations of one-dimensional monoatomic chain is given in Figure 1.1.

The total energy of a one-dimensional array of particles can be written as the summation of the kinetic energy and the potential energy (Ziman (2001)),

$$H = \frac{1}{2}\sum_{i}^{N} m_i \dot{x}^2 + U(x_1, x_2, \cdots, x_N) \tag{1.2}$$

For a one-dimensional chain with first nearest neighbor interaction, the potential energy is given in terms of a function of nearest neighbor distances by,

$$U(x_1, x_2, \cdots, x_N) = \sum_{i=1}^{N-1} f(x_i - x_{i+1}) \tag{1.3}$$

The potential energy can be defined in terms of the displacements of atoms with respect to the lattice points.

Suppose we have a one-dimensional lattice with a lattice constant a,

$$u_n = x_n - na \tag{1.4}$$

$$u_n - u_{n+1} = x_n - na - x_{n+1} + (n+1)a \tag{1.5}$$

$$= x_n - x_{n+1} + a \tag{1.6}$$

where u_n is the displacement vector of n^{th} atom. At equilibrium configuration, there is no net force on the system, so $F = -\sum_n \mathrm{d}V/\mathrm{d}x_n|_{x_n=na} = 0$ (Mahan (2010)), implying that $\mathrm{d}V/\mathrm{d}u_n|_{u_n=0} = 0$. So the potential can be approximated harmonically by using the first nonzero term in the Taylor series as below,

$$V(u_1, u_2, \cdots, u_N) = V_0 + \frac{1}{2}\sum_{ij} u_i u_j \left.\frac{\partial^2 V}{\partial u_i \partial u_j}\right|_{u_i=u_j=0} \tag{1.7}$$

$$= V_0 + \frac{1}{2}\sum_{ij} T_{ij} u_i u_j \tag{1.8}$$

where V_0 is the ground state energy, and T_{ij} is defined by,

$$T_{ij} = \left.\frac{\partial^2 V}{\partial u_i \partial u_j}\right|_{u_i=u_j=0} \tag{1.9}$$

Classical solution for the equation of motion is given by Hooke's law for an harmonic os-

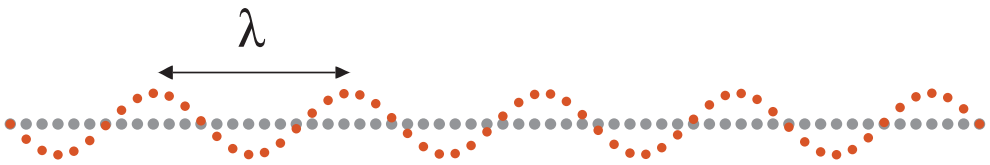

Figure 1.1. Transverse vibrations of one-dimensional monoatomic chain, each of the atoms has the same mass m and each bond corresponds to the same force constant K. Equilibrium positions, or lattice points of an unperturbed system is shown with gray dots, while the actual positions are shown by red dots. The collection of these vibrations make up a wave with a wavelength λ.

cillator where T_{ij} are the force constants implying the strength of the vibration. Hooke's law for each particle in an infinite mono-atomic chain can be defined by (Srivastava (1990)),

$$m\omega^2 u_n = 2Ku_n - Ku_{n-1} - Ku_{n+1} \tag{1.10}$$

where K is the force constant between nearest neighbor displacements. In general, for different masses and force constants, the equation of motion for each particle has the form,

$$-m_n\omega^2 u_n = K_{n,n+1}(u_{n+1} - u_n) - K_{n-1,n}(u_n - u_{n-1}) \tag{1.11}$$

In general, mass-normalized coordinates are used where $u_j \to u_j\sqrt{m_j}$, $T_{ij} \to \frac{1}{\sqrt{m_i m_j}}T_{ij}$. This is an eigenvalue problem where eigenstates represent displacements, eigenvalues correspond to different modes of oscillation, and the matrix to be diagonalized is called dynamical matrix.

1.2.2. Quantum Mechanical Harmonic Oscillator

A quantum-mechanical approach starts by defining these vibrations as a collection of quantized particles called phonons each of which is an independent simple harmonic oscillator. The Hamiltonian of a harmonic oscillator is given by (Wang et al. (2013)),

$$H = \frac{1}{2m}p^2 + \frac{1}{2}Kx^2 \tag{1.12}$$

with the definition $K = m\omega^2$ the Hamiltonian for a quantum harmonic oscillator in mass normalized coordinates ($u \to x\sqrt{m}$) is,

$$\widehat{H} = \frac{1}{2}\hat{p}^2 + \frac{1}{2}\omega^2\hat{u}^2 \tag{1.13}$$

$$= \hbar\omega\left(\hat{a}^\dagger\hat{a} + \frac{1}{2}\right) \tag{1.14}$$

In bra-ket notation, the ladder operators transform a harmonic oscillator eigenstate into a higher energy or lower energy eigenstate such that,

$$\hat{a}\,|n\rangle = \sqrt{n}\,|n-1\rangle \tag{1.15}$$

$$\hat{a}^\dagger\,|n\rangle = \sqrt{n+1}\,|n+1\rangle \tag{1.16}$$

where creation ($\hat{a}$) and annihilation ($\hat{a}^\dagger$) operators are defined by,

$$\hat{a} = \sqrt{\frac{\omega}{2\hbar}}\hat{u} + i\frac{1}{\sqrt{2\hbar\omega}}\hat{p} \tag{1.17}$$

$$\hat{a}^\dagger = \sqrt{\frac{\omega}{2\hbar}}\hat{u} - i\frac{1}{\sqrt{2\hbar\omega}}\hat{p} \tag{1.18}$$

such that the position and momentum operators are,

$$\hat{u} = \sqrt{\frac{\hbar}{2\omega}}(\hat{a}^\dagger + \hat{a}) \tag{1.19}$$

$$\hat{p} = i\sqrt{\frac{\hbar\omega}{2}}(\hat{a}^\dagger - \hat{a}) \tag{1.20}$$

The expectation value of the Hamiltonian becomes,

$$E_n = \langle n|\widehat{H}|n\rangle = \hbar\omega\left(\hat{n} + \frac{1}{2}\right) \tag{1.21}$$

$$n = \langle n|\hat{n}|n\rangle \tag{1.22}$$

where $\hat{n}$ is the number operator given by $\hat{n} = \hat{a}^\dagger\hat{a}$. In phonon picture, it corresponds to the number of phonons related to a displacement and $\hat{a}$ and $\hat{a}^\dagger$ are called phonon creation and annihilation operators. As one can see in the last equation, the system has discrete energy levels each of which differ from each other by a quantum of energy $\hbar\omega$.

1.2.3. Phonons

To describe phonons as a collection of quantum harmonic oscillators, normal coordinates are defined for each displacement and momentum operators u_n and p_n in terms of fourier series of displacement operators corresponding to each wavenumber k in 1D (or wavevector in higher dimensions) by (Mahan (2000)),

$$\hat{u}_n = \frac{1}{\sqrt{N}}\sum_k \exp(ikan)\hat{u}_k, \tag{1.23}$$

$$\hat{p}_n = \frac{1}{\sqrt{N}}\sum_k \exp(-ikan)\hat{p}_k \tag{1.24}$$

and each u_k,p_k as,

$$\hat{u}_k = \frac{1}{\sqrt{N}}\sum_n \exp(-ikan)\hat{u}_n, \tag{1.25}$$

$$\hat{p}_k = \frac{1}{\sqrt{N}}\sum_n \exp(ikan)\hat{p}_n \tag{1.26}$$

where the periodicity of the lattice implies that $\exp(ikaN) = 1$, where N is the number of displacements. Since there are N atoms in the unit cell, $k = 2\pi/(Na)$. The commutation relation between the operators of different atomic indices,

$$[\hat{u}_n, \hat{u}_m] = 0, \tag{1.27}$$

$$[\hat{p}_n, \hat{p}_m] = 0, \tag{1.28}$$

$$[\hat{u}_n, \hat{p}_m] = i\hbar\delta_{nm} \tag{1.29}$$

These relations can be expressed in the space of wave vectors,

$$[\hat{u}_k, \hat{u}_{k'}] = \frac{1}{N}\sum_{n,n'} \exp(-ikan - ik'an')[u_n, u_{n'}] \tag{1.30}$$

$$= 0 \tag{1.31}$$

since $[u_n, u_{n'}] = 0$.

Similarly $[p_n, p_{n'}] = 0$. The third relation,

$$[\hat{u}_k, \hat{p}_{k'}] = \frac{1}{N}\sum_{n,n'} \exp(-ikan + ik'an')[u_n, p_{n'}] \tag{1.32}$$

$$= \frac{1}{N}\sum_{n,n'} \exp(-ikan + ik'an')i\hbar\delta_{n,n'} \tag{1.33}$$

$$= i\hbar\frac{1}{N}\sum_{n,n'} \exp(-i(k-k')an) \tag{1.34}$$

$$= i\hbar\ \delta_{k,k'} \tag{1.35}$$

The harmonic potential for a monoatomic chain can be written as,

$$\frac{1}{2}K\sum_n(\hat{u}_n - \hat{u}_{n+1})^2 = \frac{1}{2}K\sum_n(\hat{u}_n\hat{u}_n - \hat{u}_{n+1}\hat{u}_n - \hat{u}_n\hat{u}_{n+1} + \hat{u}_{n+1}\hat{u}_{n+1}) \tag{1.36}$$

where K is the force constant between nearest-neighbor atoms. To write the potential in the wave vector space,

$$\sum_n \hat{u}_{n+m}\hat{u}_{n+s} = \sum_{k,k'} \exp(ikam)\exp(ik'as)\hat{u}_k\hat{u}_{k'}\ \frac{1}{N}\sum_n \exp(ian(k+k')) \tag{1.37}$$

$$= \sum_{k,k'} \exp(ikam)\exp(ik'as)\hat{u}_k\hat{u}_{k'}\delta_{k',-k} \tag{1.38}$$

$$= \sum_k \hat{u}_k\hat{u}_{-k}\exp(ika(m-s)) \tag{1.39}$$

where the delta function is given by,

$$\delta(x-a) = \frac{1}{N}\sum_n^N \exp(i(x-a)) \tag{1.40}$$

by using (1.39), (1.36) can be given by,

$$\frac{1}{2}K\sum_n(\hat{u}_n - \hat{u}_{n+1})^2 = \frac{1}{2}K\sum_k \hat{u}_k\hat{u}_{-k}(2 - \exp(ika) - \exp(-ika)) \tag{1.41}$$

$$= \sum_k K(1-\cos(ka))\hat{u}_k\hat{u}_{-k} \tag{1.42}$$

The solution can be simplified further, consider the classical equation of motion given in equation 1.10,

$$\omega^2 u_n = K(2u_n - u_{n-1} - u_{n+1}) \tag{1.43}$$

By assuming that the solution has a form given by (Mahan (2000)),

$$u_n = u_0\cos(kan) \tag{1.44}$$

$$= \frac{1}{2}u_0^+\exp(ikan) + \frac{1}{2}u_0^-\exp(-ikan) \tag{1.45}$$

we obtain,

$$u_{n+1} = \frac{1}{2}u_0^+ \exp(ikan)\exp(ika) + \frac{1}{2}u_0^- \exp(-ikan)\exp(-ika) \tag{1.46}$$

$$u_{n-1} = \frac{1}{2}u_0^+ \exp(ikan)\exp(-ika) + \frac{1}{2}u_0^- \exp(-ikan)\exp(+ika) \tag{1.47}$$

$$u_{n+1} + u_{n-1} = 2\cos(ka)u_n \tag{1.48}$$

$$\omega_k^2 u_n = 2K(1-\cos(ka))u_n \tag{1.49}$$

The last equation can be written in the form,

$$\omega_k^2 = 2K(1-\cos(ka)) \tag{1.50}$$

which is called a dispersion relation. By using the dispersion relation, the potential can be written in terms of frequency ω_k,

$$\frac{1}{2}K\sum_n(\hat{u}_n - \hat{u}_{n+1})^2 = \sum_k K(1-\cos(ka))\hat{u}_k\hat{u}_{-k} \tag{1.51}$$

$$= \frac{1}{2}\sum_n \omega_k^2\hat{u}_k\hat{u}_{-k} \tag{1.52}$$

The kinetic energy term,

$$\frac{1}{2}\sum_n p_n^2 = \frac{1}{2}\sum_{k,k'}\hat{p}_k\hat{p}_{k'}\frac{1}{N}\sum_n \exp(ian(k+k')) \tag{1.53}$$

$$= \frac{1}{2}\sum_{k,k'}\hat{p}_k\hat{p}_{k'}\delta_{k',-k} \tag{1.54}$$

$$= \frac{1}{2}\sum_k \hat{p}_k\hat{p}_{-k} \tag{1.55}$$

The total Hamiltonian becomes,

$$\widehat{H} = \frac{1}{2}\sum_k(\hat{p}_k\hat{p}_{-k} + \omega_k^2\hat{u}_k\hat{u}_{-k}) \tag{1.56}$$

If two operators are defined in the form similar to those given by (Kittel and Kahn (1965)),

$$\hat{a}_k = \alpha_k\hat{u}_k + i\beta_k\hat{p}_{-k} \tag{1.57}$$

$$\hat{a}_k^\dagger = \alpha_k\hat{u}_{-k} - i\beta_k\hat{p}_k \tag{1.58}$$

where α_k and β_k are k dependent constants. So,

$$\sum_k \hat{a}_k^\dagger\hat{a}_k = \sum_k(\alpha_k^2\hat{u}_{-k}\hat{u}_k + \beta_k^2\hat{p}_k\hat{p}_{-k} - i\alpha_k\beta_k(\hat{p}_k\hat{u}_k - \hat{u}_{-k}\hat{p}_{-k})) \tag{1.59}$$

since the summation is over $-\infty$ to ∞, the terms below can be collected under the same summation,

$$\sum_k \hat{a}_k^\dagger \hat{a}_k = \sum_k (\alpha_k^2 \hat{u}_k \hat{u}_{-k} + \beta_k^2 \hat{p}_k \hat{p}_{-k} + i\alpha_k \beta_k [\hat{u}_k, \hat{p}_k]) \tag{1.60}$$

$$= \sum_k (\alpha_k^2 \hat{u}_k \hat{u}_{-k} + \beta_k^2 \hat{p}_k \hat{p}_{-k} - \hbar \alpha_k \beta_k) \tag{1.61}$$

by letting $\alpha_k = \sqrt{\frac{\omega_k}{2\hbar}}$ and $\beta_k = \sqrt{\frac{1}{2\hbar\omega_k}}$, we have

$$\widehat{H} = \sum_k \hbar\omega_k \left(\hat{a}_k^\dagger \hat{a}_k + \frac{1}{2} \right) \tag{1.62}$$

with

$$\hat{a}_k = \sqrt{\frac{\omega_k}{2\hbar}} \hat{u}_k + i \sqrt{\frac{1}{2\hbar\omega_k}} \hat{p}_{-k} \tag{1.63}$$

$$\hat{a}_k^\dagger = \sqrt{\frac{\omega_k}{2\hbar}} \hat{u}_{-k} - i \sqrt{\frac{1}{2\hbar\omega_k}} \hat{p}_k \tag{1.64}$$

position and displecement operators of each wavenumber k are given by,

$$\hat{u}_k = \sqrt{\frac{\hbar}{2\omega_k}} (\hat{a}_k + \hat{a}_{-k}^\dagger) \tag{1.65}$$

$$\hat{p}_k = -i \sqrt{\frac{\hbar\omega_k}{2}} (\hat{a}_{-k} - \hat{a}_k^\dagger) \tag{1.66}$$

The operator $\hat{n}_k = \hat{a}_k^\dagger \hat{a}_k$ is called the number operator and it corresponds to the number of phonons that have a wavenumber k. In equilibrium, Bose-Einstein distribution function gives the number of phonons oscillating a specific frequancy ω_k at a temperature T (Wang et al. (2013)),

$$\langle \hat{n}_k \rangle = f_{\mathrm{BE}}(\omega_k, \mathrm{T}) = \frac{1}{e^{\beta\hbar\omega_k} - 1} \tag{1.67}$$

where $\langle \cdots \rangle$ corresponds to a trace over density matrix $\mathrm{Tr}[\hat{\rho} \cdots]$. The canonical density operator is given by,

$$\hat{\rho} = \frac{e^{-\beta \widehat{H}}}{\mathrm{Tr}\left(e^{-\beta \widehat{H}} \right)} \tag{1.68}$$

where $\beta = (k_{\mathrm{B}}\mathrm{T})^{-1}$, so the expectation values of any operator $\widehat{A}$ are evaluated as

$$\langle A \rangle = \mathrm{Tr}(\rho \widehat{A}) \tag{1.69}$$

where $\hat{n}$ is the number operator obeying the definitions below,

$$\langle \hat{a}^\dagger \hat{a} \rangle = f_{\mathrm{BE}}(\omega, \mathrm{T}) = \langle \hat{n} \rangle \tag{1.70}$$

$$\langle \hat{a} \hat{a}^\dagger \rangle = 1 + f_{\mathrm{BE}}(\omega, \mathrm{T}) = 1 + \langle \hat{n} \rangle \tag{1.71}$$

which allows us to write a commutation relation $[\hat{a}, \hat{a}^\dagger]$ as,

$$\langle [\hat{a}, \hat{a}^\dagger] \rangle = \langle \hat{a}\hat{a}^\dagger - \hat{a}^\dagger \hat{a} \rangle = 1 \tag{1.72}$$

hence $[\hat{a}, \hat{a}^\dagger] = 1$. The total energy is given by (Hofmann (2015)),

$$\langle E \rangle = \int_0^\infty \mathrm{d}\omega \, \hbar\omega \, \mathcal{D}(\omega) \left(f_{\mathrm{BE}}(\omega, \mathrm{T}) + \frac{1}{2} \right) \tag{1.73}$$

where $\mathcal{D}(\omega)$ is the density of states at ω defined by,

$$\mathcal{D}(\omega) = \frac{\mathrm{d}\mathcal{N}}{\mathrm{d}\omega} \tag{1.74}$$

where $\mathcal{N}$ is the number of modes. In a one-dimensional periodic lattice, the number of vibrational modes is equal to the number of atoms in a unit cell or supercell. If there is a non-periodic 1-d chain with N atoms, then there will be N-1 real positive eigenvalues and a zero eigenvalue which corresponds to a translation in the longitudinal axis.

For a fixed length $L = Na$ containing N atoms, wavenumber k can have discrete values (Kittel (2005)),

$$k = \mathcal{N} \frac{\pi}{L} \tag{1.75}$$

The density of states,

$$\mathcal{D}(\omega) = \frac{1}{L} \frac{\mathrm{d}\mathcal{N}}{\mathrm{d}k} \frac{\mathrm{d}k}{\mathrm{d}\omega} \tag{1.76}$$

$$= \frac{1}{\pi} \left(\frac{\mathrm{d}\omega}{\mathrm{d}k} \right)^{-1} \tag{1.77}$$

By using the dispersion relation (1.50) we can calculate the derivative $\mathrm{d}\omega/\mathrm{d}k$,

$$2\omega \frac{\mathrm{d}\omega}{\mathrm{d}k} = 2Ka \sin(ka) \tag{1.78}$$

$$\frac{\mathrm{d}\omega}{\mathrm{d}k} = \frac{Ka}{\omega} \sin(ka) \tag{1.79}$$

By using trigonometric identities on dispersion relation, we have

$$1 - \frac{\omega^2}{2K} = \cos(ka) = 1 - 2\sin^2\left(\frac{ka}{2}\right) = 2\cos^2\left(\frac{ka}{2}\right) - 1 \tag{1.80}$$

so that we have,

$$\sin\left(\frac{ka}{2}\right) = \left(\frac{\omega^2}{4K}\right)^{1/2} \tag{1.81}$$

$$\cos\left(\frac{ka}{2}\right) = \left(1 - \frac{\omega^2}{4K}\right)^{1/2} \tag{1.82}$$

hence,

$$\frac{\mathrm{d}\omega}{\mathrm{d}k} = \frac{Ka}{\omega}\sin(ka) = \frac{Ka}{\omega}2\sin\left(\frac{ka}{2}\right)\cos\left(\frac{ka}{2}\right) \tag{1.83}$$

$$= \sqrt{K}a\left(1-\frac{\omega^2}{4K}\right)^{1/2} \tag{1.84}$$

then the density of states can be written as,

$$\mathcal{D}(\omega) = \frac{1}{\pi a}\left[K\left(1-\frac{\omega^2}{4K}\right)\right]^{-1/2} \tag{1.85}$$

Figure 1.2 shows DOS of a monoatomic chain computed by equation (1.85).

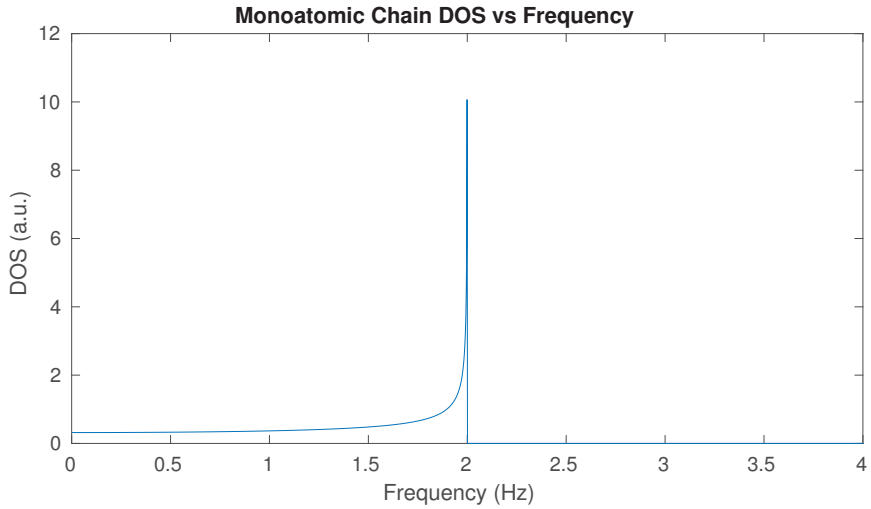

Figure 1.2. Analyttical calculation of Density of States (DOS) of a monoatomic chain by using equation (1.85) by using 2000 points between [0,4].

1.3. Anharmonicity

Harmonic approximation of the lattice potential V, allows us to determine the physics at low temperature, as it neglects any interaction between phonons. The higher order terms can be written as,

$$V(u_1,u_2,\cdots,u_N) = V_0 + \frac{1}{2}\sum_{ij} u_i u_j \left.\frac{\partial^2 V}{\partial u_i \partial u_j}\right|_0 + \frac{1}{3!}\sum_{ijk} u_i u_j u_k \left.\frac{\partial^3 V}{\partial u_i \partial u_j \partial u_k}\right|_0 + \frac{1}{4!}\sum_{ijkl} u_i u_j u_k u_l \left.\frac{\partial^4 V}{\partial u_i \partial u_j \partial u_k \partial u_l}\right|_0 + \cdots \tag{1.86}$$

where ”0” indicates that the derivatives are evaluated at equilibrium. The third order term represents the three phonon process, the forth order one represents four-phonon process, and so on. These higher order terms are temperature dependent and their contribution to the energy increases with increasing temperature.

In a perfect crystal, harmonic phonons would have infinite lifetime resulting infinite thermal conductivity; however, in real crystals, anharmonic processes and scattering from defects and boundaries reduce their lifetimes to finite values so that the thermal conductivity becomes finite (Srivastava (2006)).

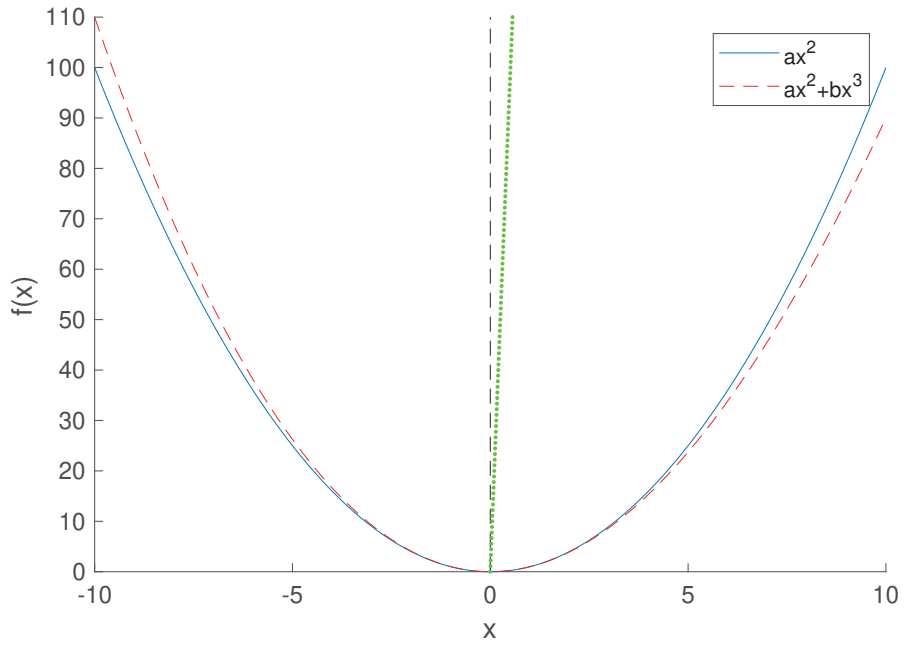

Figure 1.3. A plot of two arbitrary potentials involving 2nd and 3rd order terms in the forms ax^2 and bx^3 respectively, where $a = 1.0$ and $b = -0.01$. Effect of the bx^3 term on the equilibrium position of the harmonic potential with respect to the energy is shown with green dots. Equilibrium positions of the quadratic potential is zero for all energies.

Thermal expansion is an observable physical property of solids. Because thermal expansion is related mostly to the third order term in the potential, it is neglected in harmonic approximation. If the temperature is increased, the equilibrium point is shifted with respect to the equilibrium point at zero temperature. A simplified model for the 3rd order term is shown in Figure 1.3. The oscillation frequencies (phonon modes) are also shifted with compression or expansion and this behavior is approximated by Grüneisen parameter (Mahan (2010)).

1.4. Transport Phenomena

In this section, the basic concepts about quantum transport are represented. Most of these concepts have been introduced to the field to understand electronic transport for historical reasons, and they are valid for both electron and phonon transport in mesoscale and nanoscale systems.

Nanoscale is the length scale at the order of a nanometer, and mesoscale is defined as the length scale about the phase coherence length where quantum effects like interference, and weak localization are observed (Buot (2009)).

Depending on the system size there are three regimes of quantum transport, ballistic, diffusive and localization regimes.

1.4.1. Transport regimes

The transport is ballistic, if system size is much less than the mean free path (MFP). A classical definition for mean free path is given by the average distance between two scattering events which is proportional to the inverse lifetime of a particle. Another definition for MFP can be given in terms of the quantized conductance given by Landauer formula dependent on the transmission function τ which is equal to the number of transport channels at a frequency (in electronic transport it is a function of the energy). Number of transport channels is equal to the number of phonon (or electronic) bands available at certain frequency ω. We define mean free path as the length where transmission gets halved. Transmission function as a function of length and mean free path is given by the equation (Datta (1995)),

$$\frac{\tau_L}{\tau_0} = \frac{l_m}{l_m + L} \tag{1.87}$$

where τ_L is the transmission function of a device of length L, l_m is the mean free path. If the system size is at the order of MFP or larger, the transport is diffusive.

In general, there are multiple types of scatterings inside a crystal. Scattering with defects, grain boundaries, other particles contribute to the mean path of the particles. This is described by so called Mathiessen's Law, and it can be written for phonons as (Cahill et al. (2014)),

$$\frac{1}{\tau} = \frac{1}{\tau_u} + \frac{1}{\tau_d} + \frac{1}{\tau_b} \cdots \tag{1.88}$$

where τ_u, τ_d, τ_b correspond to the lifetimes due to umklapp scattering, defect scattering, grain boundary scattering respectively.

Under strong disorder, the interference effects reduce transmission exponentially with respect to the system size, causing different phonon modes to localize at certain energies. Localization length is the measure of the reduction in transmission function. In electronic systems, this can be shown with strong Anderson disorder imposed on the hopping parameters or onsite energies in Tight-Binding model. There are several works regarding phonon localization due to mass disorder (Hopkins and Serrano (2009)),(Mendoza and Chen (2016)). Another study (Zhou et al. (2016)) shows that long-range interaction suppresses the localization caused by the mass impurities.

1.4.2. Heat Flow and Fourier's Law

When a material is subjected to a temperature gradient between a hot and a cold reservoirs, the phonons start moving from the hot end to the cold end. After waiting long enough, the system reaches steady state, which allows us to determine transport properties of the system. A representation of a one-dimensional model system is given in Figure 1.4.

Figure 1.4. An example of a partitioned one-dimensional model for heat transport under a temperature gradient. The temperature gradient is shown by a color gradient from hot reservoir (Left region) to cold reservoir (Right region) through the device (Center region)

Reservoirs which are semi-infinitely long and in equilibrium. For a macroscopic system which is classical, Fourier's Law gives the thermal conductivity under a thermal gradient (Cahill et al. (2003)),

$$J = -\kappa_{\mathrm{th}} \nabla \mathrm{T} \tag{1.89}$$

where J is the heat flux, T is the temperature, and κ_{th} is the thermal conductivity. The negative sign indicates the flux is in the reverse direction with respect to the temperature gradient.

As discussed by Cahill (Cahill et al. (2003)), for out of equilibrium systems one should define local temperature which changes region to region, instead of defining a global temperature. For macroscopic systems which are very large, one can define local temperature for each region of space. But for nanoscale systems, the definition of such local temperature for a region is closely related to the average phonon mean free path (MFP) at that region, because MFP is a function of frequency (Cahill et al. (2003)). For three phonon Umklapp process, the phonon MFP is proportional to inverse of the squared frequency ($l_{3\mathrm{ph}} \propto \omega^{-2}$), while the MFP due to defects is proportional to $l_d = \omega^{-4}$ (Ohno (1999)).

1.4.3. Landauer Formula

For an electronic system, when the system size is large enough, Ohm's law holds for a one-dimensional wire,

$$\mathcal{G} \propto \frac{\sigma}{L} \tag{1.90}$$

where $\mathcal{G}$ is the electrical conductance, σ is the electrical conductivity and L is the length of the wire. But Ohm's law does not hold if the system is much smaller than the phase coherence length. In this case, the conductance is given by Landauer Formula. Assuming that transmission function is independent of energy, the quantized conductance for single-channel is given by (Datta (1995)),

$$\mathcal{G} = \frac{2e^2}{h}\tau \tag{1.91}$$

where τ is the transmission function, h is the Planck's constant, and $2e^2/h$ is the electrical conductance quantum. Conductance $\mathcal{G}$ is a function of energy, or frequency in phononic systems. The thermal conductance quantum is $\pi^2 k_{\mathrm{B}}^2 T/3h$ (Zhang (2015)).

For single channel, transmission function is equal to the transmission probability. The transmission probability is at its maximum value ($\tau = 1$) when there is no scattering. For multiple channels, it is given by the sum over transmission probabilities at different channels (Zhang (2015)),

$$\tau(\omega) = \sum_n \tau_n(\omega) \tag{1.92}$$

where $\tau_n(\omega)$ is the transmission probability related to each channel at frequency ω. In ballistic regime,

$$\tau(\omega) = N(\omega) \tag{1.93}$$

where $N(\omega)$ is the number channels at frequency ω.

1.5. A note on the units of force constants

For the force constants of n^{th} order, we take $[K_n] = \text{eV}/\text{Å}^{\text{n}}$. Converting to the mass-normalized coordinates, the equation of motion for a monoatomic chain is,

$$m\omega^2 x = -\frac{\mathrm{d}V}{\mathrm{d}x} \tag{1.94}$$

$$m\omega^2 x = K_1 + K_2 x + K_3 x^2 + K_4 x^3 + \cdots \tag{1.95}$$

$$\sqrt{m}\omega^2 u = K_1 + m^{1/2} K_2 u + m K_3 u^2 + m^{3/2} K_4 u^3 + \cdots \tag{1.96}$$

$$\omega^2 u = K_1 m^{-1/2} + m^{-1} K_2 u + m^{-3/2} K_3 u^2 + m^{-2} K_4 u^3 + \cdots \tag{1.97}$$

$$\omega^2 u = K_1' + K_2' u + K_3' u^2 + \cdots \tag{1.98}$$

and one can determine that

$$K_n' = m^{-n/2} K_n \tag{1.99}$$

hence the units of K_n' is given by,

$$[K_n'] = \text{eV Å}^{-\text{n}}\ \text{kg}^{-\text{n}/2} \tag{1.100}$$

CHAPTER 2

METHODS

2.1. Green Functions

Non-equilibrium Green Functions are used to determine the physics of both equilibrium and nonequilibrium systems. Equilibrium systems are those which are in thermodynamic equilibrium with reservoirs. For both equilibrium and non-equilibrium case, reservoir couplings are considered as a perturbation and Dyson equation for this perturbation can be expressed in the form of reservoir self-energies. In this section, definitions of Green function method are given for mostly for equilibrium systems. We mainly follow the formulation given by Wang et al. (2013) for both equilibrium and non-equilibrium systems.

In general, there are six Green functions in total: lesser, greater, time ordered, anti-time ordered, retarded and advanced. The greater and the lesser Green functions are given by,

$$g^{>}(t,t') = -\frac{i}{\hbar}\left\langle \hat{u}(t)\hat{u}(t')\right\rangle , \tag{2.1}$$

$$g^{<}(t,t') = -\frac{i}{\hbar}\left\langle \hat{u}(t')\hat{u}(t)\right\rangle = g^{>}(t',t). \tag{2.2}$$

where $\hat{u}(t)$ are the displacements as field operators, t, and t' are time variables. The time-ordered and anti-time ordered Green functions are given by,

$$g^{\mathrm{t}}(t,t') = -\frac{i}{\hbar}\left\langle \widehat{T}\hat{u}(t)\hat{u}(t')\right\rangle . \tag{2.3}$$

$$g^{\bar{t}}(t,t') = -\frac{i}{\hbar}\left\langle \widehat{\overline{T}}\hat{u}(t)\hat{u}(t')\right\rangle \tag{2.4}$$

where $\widehat{T}$ is the time ordering operator which orders succeeding operators in ascending time, and $\widehat{\overline{T}}$ is the anti-time ordering operator which orders succeeding operators in descending time. The the time-ordered Green function can be expressed in terms of lesser and greater Green functions as,

$$g^{\mathrm{t}}(t,t') = \theta(t-t')g^{>}(t,t') + \theta(t'-t)g^{<}(t,t'). \tag{2.5}$$

where $\theta(t)$ is the Heaviside step function given by,

$$\theta(t) = \begin{cases} 1 & t \geq 0 \\ 0 & t < 0 \end{cases} \tag{2.6}$$

In a similar way, anti-time ordered Green functions can be defined by,

$$g^{\bar{t}}(t,t') = \theta(t'-t)g^{>}(t,t') + \theta(t-t')g^{<}(t,t'), \tag{2.7}$$

There are two more important Green functions called retarded and advanced Green functions which are given by,

$$g^{\mathrm{r}}(t,t') = -\frac{i}{\hbar}\theta(t-t')\left\langle [u(t),u(t')]\right\rangle, \tag{2.8}$$

$$g^{\mathrm{a}}(t,t') = \frac{i}{\hbar}\theta(t'-t)\left\langle [u(t),u(t')]\right\rangle, \tag{2.9}$$

$$\tag{2.10}$$

Retarded Green function allows us to compute observable quantities such as dielectric susceptibility in a dielectric material, and density of states. In classical physics, it corresponds to the equation (Wang et al. (2013)),

$$\ddot{g}^{r}(t) + \omega^2 g^{r}(t) = -\delta(t) \tag{2.11}$$

To obtain steady-state transport properties, the Green functions are defined as functions of frequency by calculating their Fourier transform,

$$g^{\mathrm{r}}(\omega) = \int_{-\infty}^{\infty} g^{\mathrm{r}}(t)\mathrm{e}^{i\omega t}\mathrm{d}t, \tag{2.12}$$

$$g^{\mathrm{r}}(t) = \int_{-\infty}^{\infty} \frac{\mathrm{d}\omega}{2\pi} g^{\mathrm{r}}(\omega)\mathrm{e}^{-i\omega t}. \tag{2.13}$$

The six Green functions are related to each other with the following equations,

$$g^{\mathrm{t}} + g^{\bar{\mathrm{t}}} = g^{>} + g^{<}, \tag{2.14}$$

$$g^{\mathrm{r}} - g^{\mathrm{a}} = g^{>} - g^{<}, \tag{2.15}$$

$$g^{\mathrm{r}} + g^{\mathrm{a}} = g^{\mathrm{t}} - g^{\bar{\mathrm{t}}}, \tag{2.16}$$

where $g^{r}(\omega) = (g^{a}(\omega))^{\dagger}$. These equations hold both in time and frequency space.

2.1.1. Single Particle Green Function

For a non-interacting particle, one can evaluate the retarded Green function. The time dependence of of an operator $\widehat{A}$ in Heisenberg picture are given by (Sakurai and

Napolitano (2010)),

$$\frac{\mathrm{d}\widehat{A}}{\mathrm{d}t} = -\frac{i}{\hbar}[\widehat{A}, \widehat{H}] \tag{2.17}$$

where $\widehat{H}$ is the Hamiltonian operator. The time evolution of the annihilation operator can be calculated as below,

$$-\frac{i}{\hbar}[\hat{a}, \widehat{H}] = \left[\hat{a}, \hbar\omega\left(\hat{a}^\dagger\hat{a} + \frac{1}{2}\right)\right] \tag{2.18}$$

By using the identity,

$$[A, BC] = [A, B]C + B[A, C] \tag{2.19}$$

the time evolution of $\hat{a}$ becomes,

$$\frac{\mathrm{d}\hat{a}}{\mathrm{d}t} = -\frac{i}{\hbar}(\hbar\omega[\hat{a}, \hat{a}^\dagger]\hat{a} + \hbar\omega\hat{a}^\dagger[\hat{a}, \hat{a}]) \tag{2.20}$$

$$= -i\omega \tag{2.21}$$

Here, the identity $[\hat{a}, \hat{a}^\dagger] = 1$ is used shown in Section 1.2. Similarly, for creation operator $\hat{a}^\dagger$,

$$\frac{\mathrm{d}\hat{a}^\dagger}{\mathrm{d}t} = -\frac{i}{\hbar}(\hbar\omega[\hat{a}^\dagger, \hat{a}^\dagger]\hat{a} - \hbar\omega\hat{a}^\dagger[\hat{a}, \hat{a}^\dagger]) \tag{2.22}$$

$$= i\omega \tag{2.23}$$

and finally, the operators can be written in Heisenberg picture as,

$$\hat{a}(t) = \hat{a}_0 \exp(-i\omega t) \tag{2.24}$$

$$\hat{a}^\dagger(t) = \hat{a}_0^\dagger \exp(i\omega t) \tag{2.25}$$

where $\hat{a}_0$ and $\hat{a}_0^\dagger$ are the operators in Schrödinger picture. By using these operators, single particle retarded Green function can be expressed as (Wang et al. (2013)),

$$g^r(t, t') = -\frac{i}{\hbar}\theta(t - t')\left\langle[u(t), u(t')]\right\rangle \tag{2.26}$$

$$= -\frac{i}{\hbar}\theta(t - t')\left\langle\frac{\hbar}{2\omega}\hat{a}_0^\dagger\hat{a}\exp(i\omega(t - t')) - \frac{\hbar}{2\omega}\hat{a}_0^\dagger\hat{a}_0\exp(-i\omega(t - t'))\right\rangle$$

$$+ \left\langle\frac{\hbar}{2\omega}\hat{a}_0\hat{a}^\dagger\exp(i\omega(t - t')) - \frac{\hbar}{2\omega}\hat{a}_0\hat{a}_0^\dagger\exp(-i\omega(t - t'))\right\rangle \tag{2.27}$$

$$= -i\theta(t - t')\frac{i}{\omega}\sin(\omega(t - t'))f_{\mathrm{BE}}(\omega)$$

$$- i\theta(t - t')(1 + f_{\mathrm{BE}}(\omega))\left(-\frac{i}{\omega}\right)\sin(\omega(t - t')) \tag{2.28}$$

$$= -i\theta(t - t')\frac{\sin(\omega(t - t'))}{\omega} \tag{2.29}$$

In frequency domain,

$$g^r(\omega') = \int_{-\infty}^{\infty} \mathrm{d}t\; g^r(t) \exp(i\omega' t) \tag{2.30}$$

$$g^r(\omega') = -\int_{-\infty}^{\infty} \mathrm{d}t\; \theta(t-t') \frac{\sin(\omega(t-t'))}{\omega} \exp(i\omega' t) \tag{2.31}$$

Letting $t' = 0$, and adding an infinitesimal factor $\exp(-\eta t)$ for the integration to converge,

$$g^r(\omega') = \lim_{\eta\to 0^+} \int_{-\infty}^{\infty} \mathrm{d}t\; \theta(t) \frac{\sin(\omega(t))}{\omega} \exp(i\omega' t - \eta t) \tag{2.32}$$

$$= -\lim_{\eta\to 0^+} \left\{ \int_{-\infty}^{\infty} \mathrm{d}t\; \theta(t) \frac{\exp(i(\omega' + i\eta + \omega)t)}{2i\omega} \right\} + \lim_{\eta\to 0^+} \left\{ \int_{-\infty}^{\infty} \mathrm{d}t\; \theta(t) \frac{\exp(i(\omega' + i\eta - \omega)t)}{2i\omega} \right\} \tag{2.33}$$

$$= \lim_{\eta\to 0^+} \frac{1}{2\omega} \left(\frac{1}{\omega' + i\eta - \omega} - \frac{1}{\omega' + i\eta + \omega} \right) \tag{2.34}$$

$$= \lim_{\eta\to 0^+} \frac{1}{(\omega' + i\eta)^2 - \omega^2} \tag{2.35}$$

If we expand the first term in the denominator,

$$g^r(\omega') = \lim_{\eta\to 0^+} \frac{1}{\omega'^2 + 2i\eta\omega' - \eta^2 - \omega^2} \tag{2.36}$$

as $\eta \to 0$, η^2 converges to zero faster than η, so η^2 can safely be neglected. The other term $2\omega'\eta$ becomes zero in the limit $\eta \to 0$ since $2\omega'$ is constant with respect to η. So, one can rewrite $g^{\mathrm{r}}(\omega)$,

$$g^{\mathrm{r}}(\omega') = \frac{1}{\omega'^2 - \omega^2 + i\eta} \tag{2.37}$$

The real part of $g^{\mathrm{r}}(\omega')$,

$$\mathrm{Re}\left\{g^{\mathrm{r}}(\omega')\right\} = \frac{\omega'^2 - \omega^2}{\eta^2 + (\omega'^2 - \omega^2)^2} \tag{2.38}$$

and the imaginary part,

$$\mathrm{Im}\left\{g^{\mathrm{r}}(\omega')\right\} = -\frac{\eta}{\eta^2 + (\omega'^2 - \omega^2)^2} \tag{2.39}$$

The delta function is defined by (Liu (2012)),

$$\delta(x) = \frac{1}{\pi} \lim_{\eta\to 0} \frac{\eta}{\eta^2 + x^2} \tag{2.40}$$

and the imaginary part can be defined in terms of a delta function,

$$\mathrm{Im}\{g^r(\omega')\} = -\pi\delta(\omega^2 - \omega'^2) \tag{2.41}$$

and this quantity is related to the density of states (DOS) (Zhang (2015)),

$$\mathcal{N} = \int_0^\infty \mathrm{d}(\omega^2)\, \mathcal{D}(\omega^2) \tag{2.42}$$

where $\mathcal{D}$ is DOS, and $\mathcal{N}$ is the total number of modes. In our case, since there is only one particle, there is one mode. Variables of the integral equation can be changed to express DOS as a function of frequency,

$$\mathcal{N} = \int_0^\infty 2\omega\, \mathrm{d}\omega\, \mathcal{D}(\omega^2) \tag{2.43}$$

hence,

$$\mathcal{D}(\omega) = -\frac{2\omega}{\pi}\mathrm{Im}[g^r(\omega)] \tag{2.44}$$

2.1.2. Matrix Representation

The single particle retarded Green function can be expressed as a matrix operator of displacements of each atom in a unit cell,

$$g^r(\omega) = ((\omega + i\eta)^2 I - K)^{-1} \tag{2.45}$$

where I is the identity matrix and K is the dynamical matrix which consists of the force constants of atoms. For N particles, the size of the matrix is $N \times N$, and it has N eigenvalues corresponding to different oscillation modes. For $N = 1$ it is just a number K,

$$g^r(\omega) = ((\omega + i\eta)^2 - K)^{-1} \tag{2.46}$$

where $K = \omega'^2$, and ω' can be interpreted as the angular frequency of a spring. In matrix representation, the density of states can be written as,

$$\mathcal{D}(\omega) = -\frac{2\omega}{\pi}\mathrm{Tr}\{\mathrm{Im}[g^r(\omega)]\} \tag{2.47}$$

where Tr is the matrix trace operation. Vibrational modes are identified with positive eigenvalues of K. Because eigenvalues of K correspond to squared frequencies, and negative eigenvalues correspond to imaginary frequencies which are not physical. As it can be seen in Figure 2.1, a non-periodic finite chain has a mode with zero frequency that corresponds to translational motion as mentioned in Section 1.2, and DOS is a combination of delta functions at these discrete frequencies. The calculation is performed by using the harmonic force constant determined from DFT data given by equation (3.2).

Regarding Figure 2.1, the peaks in DOS of a finite chain are described as delta functions occur from discrete eigenmodes, but it is also known that delta functions $\delta(\omega - \omega_m)$ should diverge at each oscillation mode ω_m. The reason why they do not diverge in our plot is the fact that we use a finite imaginary number $i\eta$ which is supposed to be infinitesimal. By choosing the η parameter as a relatively large value, we introduce a broadening to the peaks which are supposed to be divergent. The half-widths of these peaks are at the order of this η parameter. Frequency mesh is another factor to determine these peaks, because if the distance between two mesh points is larger than broadening, some of the singularities may not be determined.

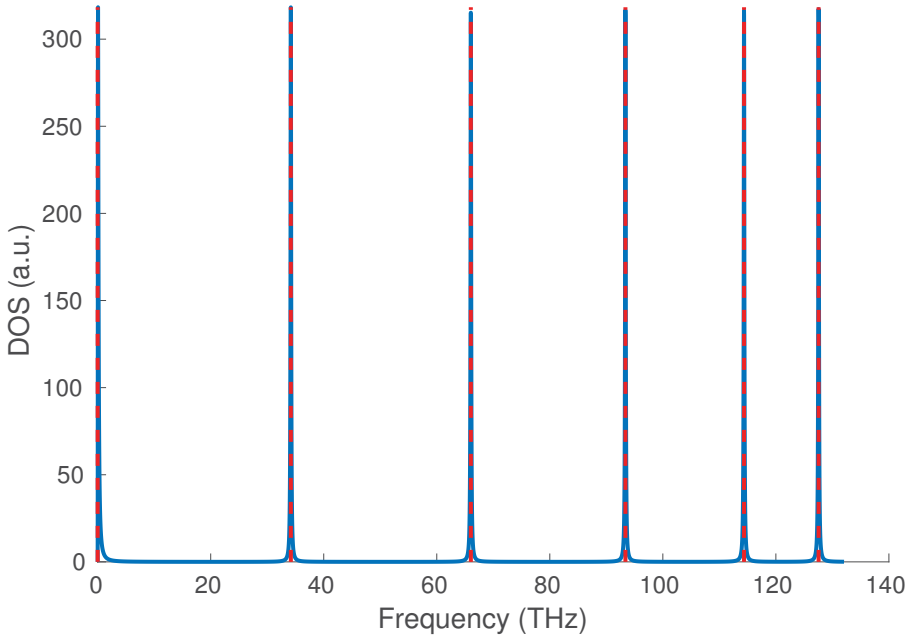

Figure 2.1. DOS as a function of frequency. DOS is shown by blue curve, and red dashed lines represent square root of eigenvalues of the dynamical matrix. $N = 6$, $K = 4.36 \times 10^{27}\text{eVÅ}^{-2}\text{kg}^{-1}$, $\eta = 10^{-3}$ and ω is sampled with 10000 points between 0 and $2\sqrt{K} = 132.06$ THz.

For a perodic unit cell, we have Bloch terms $\exp(\pm iqa)$ in the dynamical matrix, where a is the unit cell length, and q is the wavenumber. So $K_{1N}(\phi) = \exp(-i\phi)$ and $K_{N1}(\phi) = \exp(i\phi)$. So the eigenvalues of this system is a function of phase ϕ, hence DOS is needed to be integrated over all possible wavenumbers which exist in the 1$^{\text{st}}$ Brillouin zone where $\phi \in [-\pi, \pi]$,

$$\mathcal{D}(\omega) = -\frac{2\omega}{\pi}\int_{-\pi}^{\pi}\frac{\mathrm{d}\phi}{2\pi}\,\mathrm{Tr}\{\mathrm{Im}[g^r(\omega,\phi)]\} \tag{2.48}$$

$$= -\frac{2\omega}{\pi}\sum_{n}^{N_\phi}\frac{\Delta\phi}{2\pi}\,\mathrm{Tr}\{\mathrm{Im}[g^r(\omega,\phi)]\} \tag{2.49}$$

with a uniform mesh between $[-\pi,\pi]$, $\Delta\phi = 2\pi/N_\phi$, hence,

$$\mathcal{D}(\omega) = -\frac{2\omega}{\pi N_\phi}\sum_{n=1}^{N_\phi}\mathrm{Tr}\{\mathrm{Im}[g^r(\omega,\phi_n)]\} \tag{2.50}$$

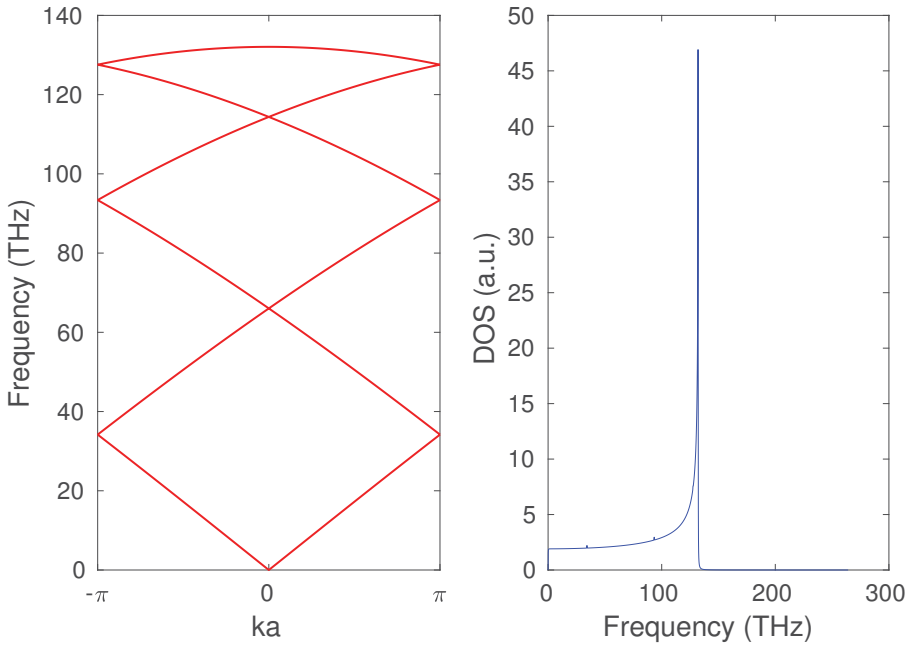

Figure 2.2. (a) 1-dimensional band structure of a 6 atom unit-cell periodic chain.(b) DOS as a function of frequency integrated over the first Brillouin zone. $N = 6$, $K = 4.36 \times 10^{27}\mathrm{eV\AA}^{-2}\mathrm{kg}^{-1}$, $\eta = 10^{-3}$, ω mesh has 2000 points between 0 and $4\sqrt{K} = 264.12$ THz, and $\phi \in [-\pi,\pi]$ sampled with 2000 points. The integral of DOS over frequency is equal to 5.99

2.1.3. Reservoir Self-Energies

In equilibrium Green functions, reservoir couplings are treated as a perturbation which allows us to write Dyson's equation in terms of uncoupled Green functions. The

main assumption is that the system is uncoupled at time $-\infty$ and the state of the uncoupled system is known. As the system evolves with time $t \to t_0$ the perturbation is switched on adiabatically, and it is switched off adiabatically as t goes to ∞. The time-evolution of the Green function with $|\phi\rangle_0$ at $t \to -\infty$, and $u(t)$ as the field operators is given by (Mahan (2000)),

$$G_{ij}(t,t') = -\frac{i}{\hbar}\frac{\langle\phi_0|\widehat{T}\, S(\infty,-\infty)\hat{u}_i(t)\hat{u}_j(t')|\phi_0\rangle}{\langle\phi_0|S(\infty,-\infty)|\phi_0\rangle} \tag{2.51}$$

where $S(t,t')$ is the S-matrix and i,j are cite indices,

$$S(t,t') = \widehat{T}\exp\left(-\frac{i}{\hbar}\int_{t'}^{t}\mathrm{d}t_1\,\widehat{V}(t_1)\right) \tag{2.52}$$

$$S(\infty,-\infty) = \sum_{n=0}^{\infty}\frac{(-i/\hbar)^n}{n!}\int_{-\infty}^{\infty}\mathrm{d}t_1\cdots\int_{-\infty}^{\infty}\mathrm{d}t_n\,\widehat{T}\,\widehat{V}(t_1)\cdots\widehat{V}(t_n) \tag{2.53}$$

where $\widehat{V}$ is the perturbation potential, $\widehat{T}$ is the time-ordering operator. If the system is in equilibrium, (2.53) is just a phase. $G_{ij}(t,t')$ can be expanded in series and the terms in the series can be represented by diagrams and one only needs to evaluate connected diagrams. The irreducible diagrams contribute to the so-called self-energy. The reservoir coupling is defined as such a self-energy expression $\Sigma(t,t')$. These relations can also be described in frequency space. Suppose we have a force constant matrix K and a coupling matrix V, the retarded Green function can be expanded in series (Hirose and Kobayashi (2014))

$$\begin{aligned} G &= (\omega^2 I - K - V)^{-1} && (2.54)\\ &= \{(\omega^2 I - K)(I - (\omega^2 I - K)^{-1}V)\}^{-1} \\ &= (I - gV)^{-1}g \\ &= g + gVg + gVgVg + \cdots && (2.55)\\ &= g + gV(g + gVg + \cdots) \\ &= g + gVG && (2.56) \end{aligned}$$

where g is the uncoupled retarded Green function, and g and G are functions of the frequency ω. We can rewrite (2.55) as,

$$\begin{aligned} G &= g + (gV + gVgV + \cdots)g \\ &= g + GVg && (2.57) \end{aligned}$$

(2.56) and (2.57) are two equivalent representations of Dyson equation. In time domain, they are given by,

$$G(t,t') = \int_{-\infty}^{\infty} \mathrm{d}t_1 g(t,t_1) V G(t_1,t') \tag{2.58}$$

$$G(t,t') = \int_{-\infty}^{\infty} \mathrm{d}t_1 G(t,t_1) V g(t_1,t') \tag{2.59}$$

The terms in (2.55) include all multiple scatterings, but we only need to evaluate irreducible diagrams that cannot be split into two parts by the cut of a single line and Dyson equation is given by (Hirose and Kobayashi (2014)),

$$G = g + g\Sigma G \tag{2.60}$$

$$G = g + G\Sigma g \tag{2.61}$$

where Σ is the retarded self energy including all irreducible diagrams. In time domain they are given by (Stefanucci and van Leeuwen (2013)),

$$G(t,t') = g(t,t') + \int_{-\infty}^{\infty} \mathrm{d}t_1 \int_{-\infty}^{\infty} \mathrm{d}t_2 \; g(t,t_1)\; \Sigma(t_1,t_2)\; G(t_2,t') \tag{2.62}$$

$$G(t,t') = g(t,t') + \int_{-\infty}^{\infty} \mathrm{d}t_1 \int_{-\infty}^{\infty} \mathrm{d}t_2 \; G(t,t_1)\; \Sigma(t_1,t_2)\; g(t_2,t') \tag{2.63}$$

The partitioned form of the Hamiltonian for the system in Figure 1.4 is given by (Wang et al. (2013)),

$$H = H_{\mathrm{L}} + H_{\mathrm{C}} + H_{\mathrm{R}} + u_{\mathrm{L}}^{\mathrm{T}} V^{\mathrm{LC}} u_{\mathrm{C}} + u_{\mathrm{R}}^{\mathrm{T}} V^{\mathrm{RC}} u_{\mathrm{C}} \tag{2.64}$$

$$= \sum_{j \in \mathrm{L,C,R}} H_j + u_{\mathrm{L}}^{\mathrm{T}} V^{\mathrm{LC}} u_{\mathrm{C}} + u_{\mathrm{R}}^{\mathrm{T}} V^{\mathrm{RC}} u_{\mathrm{C}} \tag{2.65}$$

where the the indices C, L, R correspond to the center, left and right region respectively, and,

$$H_j = \frac{1}{2} \left\{ p_j^{\mathrm{T}} p_j + u_j^{\mathrm{T}} K u_j \right\} \tag{2.66}$$

In partitioned base of L,C and R; the quadratic Hamiltonian is defined by,

$$K + V = \begin{bmatrix} K^{\mathrm{L}} & V^{\mathrm{LC}} & 0 \\ V^{\mathrm{CL}} & K^{\mathrm{C}} & V^{\mathrm{CR}} \\ 0 & V^{\mathrm{RC}} & K^{\mathrm{R}} \end{bmatrix} \tag{2.67}$$

where the coupling matrix V is defined by,

$$V = \begin{bmatrix} 0 & V^{\mathrm{LC}} & 0 \\ V^{\mathrm{CL}} & 0 & V^{\mathrm{CR}} \\ 0 & V^{\mathrm{RC}} & 0 \end{bmatrix} \tag{2.68}$$

where V^{ij} are the interactions between partitions i and j where $\mathrm{i},\mathrm{j} \in \{\mathrm{L},\mathrm{R}\}$. Note that the reservoirs are not coupled to each other. We can write the retarded Green function equation in matrix form,

$$\begin{bmatrix} \Omega^2 - K^{\mathrm{L}} & V^{\mathrm{LC}} & 0 \\ V^{\mathrm{CL}} & \Omega^2 - K^{\mathrm{C}} & V^{\mathrm{CR}} \\ 0 & V^{\mathrm{RC}} & \Omega^2 - K^{\mathrm{R}} \end{bmatrix} \begin{bmatrix} G^{\mathrm{L}} & G^{\mathrm{LC}} & G^{\mathrm{LR}} \\ G^{\mathrm{CL}} & G^{\mathrm{C}} & G^{\mathrm{CR}} \\ G^{\mathrm{RL}} & G^{\mathrm{RC}} & G^{\mathrm{R}} \end{bmatrix} = \begin{bmatrix} 1 & 0 & 0 \\ 0 & 1 & 0 \\ 0 & 0 & 1 \end{bmatrix} \tag{2.69}$$

where $\Omega = (\omega + i\eta)$, and it does not necessary for LR and RL parts of the retarded Green function to be zero. Also, r superscript is dropped. By using the second column of the identity matrix (right-hand side), the following identities are obtained (Ryndyk (2016)),

$$(\Omega^2 - K^{\mathrm{L}})G^{\mathrm{LC}} + V^{\mathrm{LC}}G^{\mathrm{C}} = 0 \tag{2.70}$$

$$V^{\mathrm{CL}}G^{\mathrm{LC}} + (\Omega^2 - K^{\mathrm{C}})G^{\mathrm{C}} + V^{\mathrm{CR}}G^{\mathrm{RC}} = 1 \tag{2.71}$$

$$V^{\mathrm{RC}}G^{\mathrm{C}} + (\Omega^2 - K^{\mathrm{R}})G^{\mathrm{RC}} = 0 \tag{2.72}$$

we solve for G^{LC} and G^{RC} in (2.70) and (2.72) respectively,

$$G^{\mathrm{LC}} = -(\Omega^2 - K^{\mathrm{L}})^{-1}V^{\mathrm{LC}}G^{\mathrm{C}} \tag{2.73}$$

$$G^{\mathrm{RC}} = -(\Omega^2 - K^{\mathrm{R}})^{-1}V^{\mathrm{RC}}G^{\mathrm{C}} \tag{2.74}$$

and these can be substituted into (2.71) to obtain,

$$\{(\Omega^2 - K^{\mathrm{C}}) - V^{\mathrm{CL}}(\Omega^2 - K^{\mathrm{L}})^{-1}V^{\mathrm{LC}} - V^{\mathrm{CR}}(\Omega^2 - K^{\mathrm{R}})^{-1}V^{\mathrm{RC}}\}G^{\mathrm{C}} = 1 \tag{2.75}$$

it means that one can write an effective dynamical matrix as,

$$\widetilde{K}^{\mathrm{C}} = K^{\mathrm{C}} + V^{\mathrm{CL}}(\Omega^2 - K^{\mathrm{L}})^{-1}V^{\mathrm{LC}} + V^{\mathrm{CR}}(\Omega^2 - K^{\mathrm{R}})^{-1}V^{\mathrm{RC}} \tag{2.76}$$

and solve the retarded Green function for this effective dynamical matrix in a similar way that it is done for the uncoupled system.

$$G^{\mathrm{C}} = (\Omega^2 - \widetilde{K}^{\mathrm{C}})^{-1} \tag{2.77}$$

These effective terms in the dynamical matrix are called reservoir self energies, defined by

$$\Sigma^{\mathrm{L}} = V^{\mathrm{CL}}g^{\mathrm{L}}V^{\mathrm{LC}} \tag{2.78}$$

$$\Sigma^{\mathrm{R}} = V^{\mathrm{CR}}g^{\mathrm{R}}V^{\mathrm{RC}} \tag{2.79}$$

where $g^{\mathrm{L/R}}$ are the uncoupled retarded Green functions of the reservoirs,

$$g^{\mathrm{L}} = (\Omega^2 - K^{\mathrm{L}})^{-1} \tag{2.80}$$

$$g^{\mathrm{R}} = (\Omega^2 - K^{\mathrm{R}})^{-1} \tag{2.81}$$

For thermalization to occur, reservoirs are choosen to be semi-infinitely long and repetitive. The exact dynamical matrices of reservoirs are supposed to be infinitely large which cannot be inverted.

Instead, one can use a numerically efficient recursive algorithm to compute these Green functions which is based on periodic nature of these reservoir unit cells (Sancho et al. (1985)). For phonon transport, a pseudo-code is given by (Wang et al. (2007)) to compute these reservoir Green functions, or Surface Green Functions (SGF).

2.1.4. Level Broadening and Transmission Function

The central region which is called the device, has a finite number of discrete energy levels when it is not coupled to the reservoirs. After the device is coupled to these ideal reservoirs and the system evolves into a steady state, these energy levels may shift and broaden due to the continuum in the reservoir states (Hirose and Kobayashi (2014)). The shift in energy levels is proportional to the real part of the retarded self-energy, and broadening (or level-width function) is given by the imaginary part of the self energy (Ryndyk (2016)),

$$\Gamma^{\mathrm{L/R}} = i\left(\Sigma^{\mathrm{L/R}} - \Sigma^{\mathrm{L/R}\dagger}\right) \tag{2.82}$$

The transmission function for these equilibrium systems is given by (Ryndyk (2016)),

$$\mathcal{T}(\omega) = \mathrm{Tr}\left[\Gamma^{\mathrm{L}} G^{\mathrm{C}} \Gamma^{\mathrm{R}} G^{\mathrm{C}\dagger}\right] \tag{2.83}$$

where all operators in the trace are functions of frequency ω.

2.1.5. An example calculation

For a semi-infinite one-dimensional reservoir with tight-binding model, the uncoupled retarded Green functions evaluated analytically by Müller et al. (2000) for electronic transport. The terms in the dynamical matrix for a chain are similar to those in tight-binding model, so Müller's formula can be written for phonon transport,

$$g^{\mathrm{s}} = -\frac{1}{k}\exp\left(i\theta\right), \qquad \theta = \cos^{-1}\left(1 - \frac{(\omega + i\eta)^2}{2k}\right). \tag{2.84}$$

where g^{s} is the Green function of reservoir "s" ($\mathrm{s} \in \{L, R\}$) called surface Green function, K is the harmonic force constant, ω is frequency as an independent parameter, and η is

the small damping factor. Assuming that there is only one atom in the device region, the retarded self-energy becomes,

$$\Sigma^{\mathrm{s}} = V^{\mathrm{Cs}} g^{\mathrm{s}} V^{\mathrm{sC}} \tag{2.85}$$

$$= -k \exp\left(i\theta\right). \tag{2.86}$$

There are two reservoirs, so it is multiplied by two and the retarded Green function of the system is,

$$G^{r}\left(\omega\right) = \left(\omega^2 - 2k - 2\Sigma^{\mathrm{s}}\right)^{-1} \tag{2.87}$$

$$= \left(\omega^2 - 2k + 2k\exp\left(i\theta\right)\right)^{-1}. \tag{2.88}$$

and DOS is given by,

$$\mathcal{D}\left(\omega\right) = -\frac{2\omega}{\pi}\mathrm{Im}\left\{\mathrm{Tr}\left[G^{r}\right]\right\}, \tag{2.89}$$

$$= -\frac{2\omega}{\pi}\mathrm{Im}\left[\left(\omega^2 - 2k + 2k\exp\left(i\theta\right)\right)^{-1}\right] \tag{2.90}$$

where η is only used in reservoirs for this model and that is enough to avoid singularities. If we rewrite (2.84) by using the definition $\Omega = \omega + i\eta$,

$$\cos(\theta) = 1 - \frac{\Omega^2}{2k} \tag{2.91}$$

$$= 2\cos^2\left(\frac{\theta}{2}\right) - 1 = 1 - 2\sin^2\left(\frac{\theta}{2}\right) \tag{2.92}$$

we have,

$$\sin\left(\frac{\theta}{2}\right) = \left(\frac{\Omega^2}{4k}\right)^{1/2} \tag{2.93}$$

$$\cos\left(\frac{\theta}{2}\right) = \left(1 - \frac{\Omega^2}{4k}\right)^{1/2} \tag{2.94}$$

so that we can rewrite the term in the paranthesis in equation (2.90) as,

$$\omega^2 + 2k(\exp(i\theta) - 1) = \omega^2 + 2k(\cos(\theta) + i\sin(\theta) - 1) \tag{2.95}$$

$$= \omega^2 + 2k\left(\cos(\theta) + 2i\sin\left(\frac{\theta}{2}\right)\cos\left(\frac{\theta}{2}\right) - 1\right) \tag{2.96}$$

$$= \omega^2 + 2k\left(-\frac{\Omega^2}{2k} + 2i\left(\frac{\Omega^2}{4k}\right)^{1/2}\left(1 - \frac{\Omega^2}{4k}\right)^{1/2}\right) \tag{2.97}$$

as $\Omega \to \omega$ we have,

$$\mathcal{D}(\omega) = \frac{1}{\pi}\left[k\left(1 - \frac{\omega^2}{4k}\right)\right]^{-1/2} \tag{2.98}$$

which is identical to the analytical formula (1.85). Broadening function is given by the imaginary part of the self-energy,

$$\Gamma_{\mathrm{s}} = i(\Sigma^{\mathrm{s}} - \Sigma^{\mathrm{s}\dagger}) \tag{2.99}$$

$$- ik(\exp(i\theta) - \exp(-i\theta)) \tag{2.100}$$

$$= 2k\sin(\theta) \tag{2.101}$$

If we expand this equation by using trigonometric identities, we obtain

$$\Gamma_{\mathrm{s}} = 4k\sin\left(\frac{\theta}{2}\right)\cos\left(\frac{\theta}{2}\right) \tag{2.102}$$

$$= 4k\left(\frac{\Omega^2}{4k}\right)^{1/2}\left(1 - \frac{\Omega^2}{4k}\right)^{1/2} \tag{2.103}$$

$$= 2\Omega\left[k\left(1 - \frac{\Omega^2}{4k}\right)\right]^{1/2} \tag{2.104}$$

in the last equation we see that we have a divergent imaginary part for $\Omega^2 > 4k$. Also, we know that broadening is real, because it is the imaginary part of the self-energy, so we can discard that imaginary part completely by re-defining the broadening as,

$$\Gamma_{\mathrm{s}} = 2k\mathrm{Re}[\sin(\theta)] \tag{2.105}$$

The transmission function is given by,

$$\mathcal{T}(\omega) = \mathrm{Tr}[\Gamma^{\mathrm{L}}(\omega)G^r(\omega)\Gamma^{\mathrm{R}}(\omega)G^a(\omega)] \tag{2.106}$$

For monoatomic chain, the functions in the trace in the last equation are just numbers, so we can rewrite transmission as,

$$\mathcal{T}(\omega) = \Gamma^{\mathrm{L}}(\omega)\Gamma^{\mathrm{R}}(\omega)G^r(\omega)G^a(\omega) \tag{2.107}$$

by using equation (2.104), we obtain

$$\Gamma^{\mathrm{L}}(\omega)\Gamma^{\mathrm{R}}(\omega) = 4\Omega^2 k\left(1 - \frac{\Omega^2}{4k}\right) \tag{2.108}$$

and by using equation (2.97), as $\Omega \to \omega$, we can write

$$G^r(\omega)G^a(\omega) = \frac{1}{4k\omega^2\left(1 - \frac{\omega^2}{4k}\right)} \tag{2.109}$$

hence,

$$\mathcal{T}(\omega) = 1, \qquad \omega^2 \leq 4k \tag{2.110}$$

By using equations (2.88) and (2.105) the transmission function can also be written as,

$$\mathcal{T}(\omega) = 4k^2 \mathrm{Re}\left[\sin^2(\theta)\right] \left|\left(\omega^2 - 2k + 2k\exp(i\theta)\right)^{-1}\right|^2 \tag{2.111}$$

For monoatomic chain, surface green function, DOS and Transmission function are shown in Figure 2.3. The calculations for Figure 2.3 are done by using equations (2.84),(2.90) and (2.111). Because SGF is proportional to the self-energy with a factor K^{-2} for this model, SGF in Figure 2.3 can be interpreted as a self-energy.

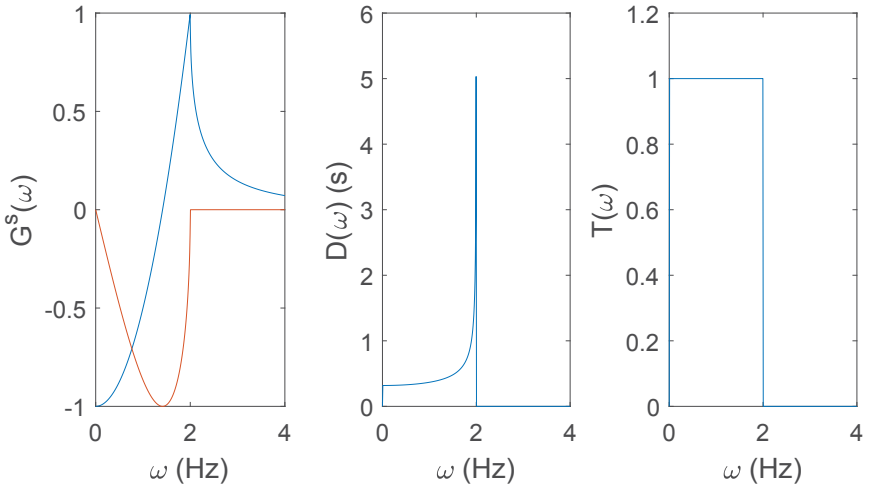

Figure 2.3. An example calculation of the SGF (a), DOS (b), and transmission function (c) for the analytical formula derived in Section 2.1.5. In (a), blue line shows the real part of the SGF, while red line shows the imaginary part. The parameters are $K = 1\mathrm{eV\ \AA^{-2}\ kg^{-1}}$,$\eta = 10^{-5}$,$\omega \in [0, 4]\mathrm{Hz}$ sampled with 500 points.

2.2. Non-equilibrium Green Functions

In this section, the basic concepts of NEGF like contour time, and operators of contour time is introduced. Then, mathematical tools like Langreth theorem is represented. In the last part of this section, heat current and conductance are represented in NEGF formalism.

2.2.1. Green Functions of Contour Time

In equilibrium systems, the perturbation is introduced slowly as $t \to t_0$, and then slowly decays as $t \to \pm\infty$. The unperturbed state of the system is known at $t \to \pm\infty$ and Gell-Mann and Low theorem states that they are equal to each other except for a phase factor (Haug and Jauho (2007)). However, in non-equilibrium systems, the perturbation does not decay as $t \to \infty$, hence the Gell-Mann and Low theorem does not hold (Zhu et al. (2016)).

Because the time-reversal symmetry is broken, the time evolution is defined on a contour which starts and ends at t_0, travels through the upper branch and the lower branch respectively. Such a contour is shown as,

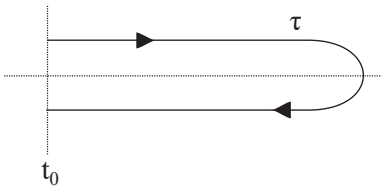

where τ is called a contour time. As stated by Wang et al. (2013), the common choices for t_0 are 0 and $-\infty$. Hirose and Kobayashi (2014) assume $t_0 \to -\infty$, and define S-Matrix by,

$$\widehat{S}(-\infty,\infty) = \widehat{T}_c \exp\left(-\frac{i}{\hbar}\int_{\mathrm{c}} \widehat{V}(\tau)\mathrm{d}\tau\right) \tag{2.112}$$

where $\hat{T}_c$ is the contour time ordering operator on a contour c. Green functions of contour time are similar to the Green functions of real time (Wang et al. (2013)),

$$g^{>}(\tau,\tau') = -\frac{i}{\hbar}\left\langle \hat{u}(\tau)\hat{u}(\tau')\right\rangle, \tag{2.113}$$

$$g^{<}(\tau,\tau') = -\frac{i}{\hbar}\left\langle \hat{u}(\tau')\hat{u}(\tau)\right\rangle = g^{>}(\tau',\tau), \tag{2.114}$$

$$g^{\mathrm{t}}(\tau,\tau') = -\frac{i}{\hbar}\left\langle \widehat{T}_{\mathrm{c}}\hat{u}(\tau)\hat{u}(\tau')\right\rangle, \tag{2.115}$$

$$g^{\bar{\mathrm{t}}}(\tau,\tau') = -\frac{i}{\hbar}\left\langle \overline{T}_{\mathrm{c}}\hat{u}(\tau)\hat{u}(\tau')\right\rangle \tag{2.116}$$

where $\hat{\overline{T}}_c$ is the contour anti-time ordering operator. Contour time τ corresponds to a real time t with a branch index σ, where $\sigma \in \{+,-\}$, (+ for upper branch, - for lower branch). The type of Green function depends where time variables exists on the contour (Mahan (2000)). If they both are at the upper (lower) branch, the Green function is contour time (anti-time) ordered. If t is at the upper (lower) branch and t' is at the lower (upper) branch, it is lesser (greater) Green function. This explains the identity in Equation 2.114. If the

time variables are replaced in lesser Green function, we obtain greater Green function and vice versa.

2.2.2. Multiple Contours and Langreth Theorem

To compute Dyson's equation, one needs to evaluate convolution of multiple operators. To express the lesser part of the Green function, this convolution is expressed as a combination of different contours. First, self-energy is considered as a Green function. Two Green functions under a convolution integral on a contour c is given by,

$$C(\tau, \tau') = \int_{\mathrm{c}} \mathrm{d}\tau_1 \; A(\tau, \tau_1) B(\tau_1, \tau') \tag{2.117}$$

the equation can be represented by a combination of contours c_1 and c_2,

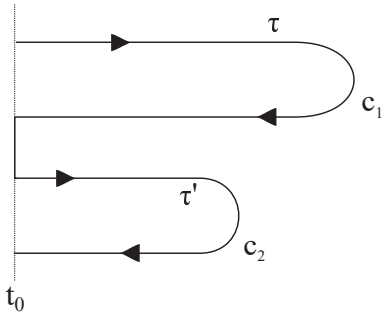

τ exists on c_1 and τ' exists on c_2 and the integral can be written as,

$$C(\tau, \tau') = \int_{\mathrm{c}_1} \mathrm{d}\tau_1 \; A(\tau, \tau_1) B(\tau_1, \tau') + \int_{\mathrm{c}_2} \mathrm{d}\tau_1 \; A(\tau, \tau_1) B(\tau_1, \tau') \tag{2.118}$$

the lesser part of the Green function becomes,

$$C^{<}(\tau, \tau') = \int_{\mathrm{c}_1} \mathrm{d}\tau_1 \; A(\tau, \tau_1) B^{<}(\tau_1, \tau') + \int_{\mathrm{c}_2} \mathrm{d}\tau_1 \; A^{<}(\tau, \tau_1) B(\tau_1, \tau') \tag{2.119}$$

Note that for the integration on c_1, we always have $\tau_1 < \tau'$. Similarly, on c_2, we always have $t < t_1$. By converting to the real time, when t, t_1 we have $A^{<}(t, t_1)$ and when $t > t_1$ we have $A^{>}(t, t_1)$. Then the right hand side can be written as (Hirose and Kobayashi (2014)),

$$A^{<}(t, t') = \int_{-\infty}^{\infty} \mathrm{d}t_1 \; \{A^{r}(t, t_1) B^{<}(t_1, t') + A^{<}(t, t_1) B^{a}(t_1, t')\} \tag{2.120}$$

Similarly,

$$A^{>}(t, t') = \int_{-\infty}^{\infty} \mathrm{d}t_1 \; \{A^{r}(t, t_1) B^{<}(t_1, t') + A^{<}(t, t_1) B^{a}(t_1, t')\} \tag{2.121}$$

which is known as Langreth theorem (Devreese (1976)). The detailed derivations of these formula are given by Hirose and Kobayashi (2014). These derivations are based on writing the integral as a summation of two; one is over $(-\infty, t]$ and the other is over $[t, \infty)$ and making use of the relations between G^r, G^a with $G^<, G^>$, and eventually taking the limit $t \to \infty$. These relations can be expressed in a symbolic form,

$$C^< = A^r B^< + A^< B^a \tag{2.122}$$

$$C^> = A^r B^> + A^> B^a \tag{2.123}$$

and the retarded part is given by (Hirose and Kobayashi (2014))

$$C^r = A^r B^r \tag{2.124}$$

similarly, the advanced Green function can be defined by,

$$C^a = A^a B^a \tag{2.125}$$

For three Green functions A, B, and C such that $D = ABC$,

$$D^< = A^r (BC)^< + A^< (BC)^a \tag{2.126}$$

$$= A^r B^r C^< + A^r B^< C^a + A^< B^a C^a \tag{2.127}$$

2.2.3. Dyson Equation

In Section 2.1.3, Dyson's equation (Equation 2.58 and 2.62) for reservoir coupling is introduced. For non-equilibrium self-energies they can be defined by,

$$G(\tau, \tau') = g(\tau, \tau') + \int_c \mathrm{d}\tau_1 g(\tau, \tau_1) V G(\tau_1, \tau') \tag{2.128}$$

$$G(\tau, \tau') = g(\tau, \tau') + \int_c \mathrm{d}\tau_1 \mathrm{d}\tau_2 \; g(\tau, \tau_1) \Sigma(\tau_1, \tau_2) G(\tau_2, \tau') \tag{2.129}$$

the lesser part can be written by using Langreth's theorem given by Equation 2.127,

$$G^< = g^< + g^r \Sigma^r G^< + g^r \Sigma^< G^a + g^< \Sigma^a G^a \tag{2.130}$$

this recursive relation can be represented in an equivalent form (Haug and Jauho (2007)),

$$G^< = (1 + G^r \Sigma^r) g^< (1 + \Sigma^a G^a) + G^r \Sigma^< G^a \tag{2.131}$$

as stated by Wang et al. (2013), for the equilibrium systems in steady state the first term is zero, so

$$G^{<} = G^{r}\Sigma^{<}G^{a} \tag{2.132}$$

in a similar way,

$$G^{>} = G^{r}\Sigma^{>}G^{a} \tag{2.133}$$

and the retarded part is simply,

$$G^{\mathrm{r}} = g^{r} + g^{\mathrm{r}}\Sigma^{\mathrm{r}}G^{\mathrm{r}} \tag{2.134}$$

For a system in equilibrium with the reservoirs, (2.132) and (2.133) reduces to the equations below,

$$G^{<}(\omega) = f_{\mathrm{BE}}(\omega)(G^{\mathrm{r}}(\omega) - G^{\mathrm{a}}(\omega)) \tag{2.135}$$

$$G^{>}(\omega) = (1 + f_{\mathrm{BE}}(\omega))(G^{\mathrm{r}}(\omega) - G^{\mathrm{a}}(\omega)) \tag{2.136}$$

The Dyson equation for all Green functions except for the time and anti-time ordered are then,

$$G^{\mathrm{r}} = g^{\mathrm{r}}(1 + \Sigma^{\mathrm{r}}G^{\mathrm{r}}) \tag{2.137}$$

$$G^{\mathrm{a}} = g^{\mathrm{a}}(1 + \Sigma^{\mathrm{a}}G^{\mathrm{a}}) \tag{2.138}$$

$$G^{>} = G^{\mathrm{r}}\Sigma^{>}G^{\mathrm{a}} \tag{2.139}$$

$$G^{<} = G^{\mathrm{r}}\Sigma^{<}G^{\mathrm{a}} \tag{2.140}$$

2.2.4. Heat Current and Conductance

In this section, we describe the heat and conductance in terms of Green functions in matrix form and we mainly follow the work by Wang et al. (2013). Heat current is defined by the rate of change in the energy in one of the reservoirs (Wang et al. (2013)),

$$I_L(t) = -\langle \frac{\mathrm{d}H_L(t)}{\mathrm{d}t} \rangle \tag{2.141}$$

$$= \langle \dot{u}_L(t)^T V^{\mathrm{LC}} u_C(t) \rangle \tag{2.142}$$

The time dependence is introduced to the system via reservoir couplings,

$$I_L(t) = i\hbar \frac{\partial}{\partial t'} \mathrm{Tr}\, \left[G^{\lessgtr}_{\mathrm{CL}}(t,t') V^{\mathrm{LC}} \right]\big|_{t'=t} \tag{2.143}$$

This leads to the following equation in frequency space,

$$I_L(t) = \int_{-\infty}^{\infty} \frac{\mathrm{d}\omega}{4\pi} \hbar\omega \, \mathrm{Tr}[G^{<}\Sigma_{\mathrm{L}}^{>} - G_{\mathrm{L}}^{>}\Sigma_{\mathrm{L}}^{<}] \tag{2.144}$$

In equilibrium, by using (2.135) and (2.136), and the relations among the Green functions the trace term can be reduced to (2.83).

Conductance in equilibrium is given by,

$$\kappa = \frac{1}{2\pi} \int_0^{\infty} \mathrm{d}\omega \, \hbar\omega \, \mathcal{T}(\omega) \frac{\mathrm{d}f(\omega, T)}{\mathrm{d}T} \tag{2.145}$$

by letting $x = x(\omega) = \hbar\omega / k_{\mathrm{B}}T$ the equation becomes,

$$\kappa = \frac{1}{2\pi} \int_0^{\infty} \left(\frac{k_{\mathrm{B}}T}{\hbar} \mathrm{d}x \right) \, k_{\mathrm{B}}T x \, \tau(x) \left(-\frac{x}{T} \right) \left(-\frac{\exp(x)}{(\exp(x)-1)^2} \right) \tag{2.146}$$

$$= \frac{k_{\mathrm{B}}^2 T}{2\pi\hbar} \int_0^{\infty} \frac{x^2 \exp(x)}{(\exp(x)-1)^2} \tau(x) \tag{2.147}$$

where τ is the transmission function. We may choose an upper limit $\omega_{\max}$ and corresponding $x_{\max}$ for the integral beyond which transmission is zero.

2.3. Anharmonic Self-Energies

Non-linear terms in the Hamiltonian can be incorporated into NEGF method in the form of self-energies corresponding to these terms. Then we can solve for G^r with an equation similar to the one with the equilibrium Green function,

$$G^r = ((\omega + i\eta)^2 I - K - \Sigma)^{-1} \tag{2.148}$$

but this time the retarded self-energy Σ corresponds to

$$\Sigma = \Sigma_{\mathrm{L}} + \Sigma_{\mathrm{R}} + \Sigma_n \tag{2.149}$$

where $\Sigma_{L/R}$ are the reservoir self-energies, and Σ_n is the self energy due to the non-linear interactions such as anharmonic coupling.

2.3.1. Diagrammatic Technique

Phonon-phonon coupling can be evaluated using diagrammatic perturbation technique. The lowest order diagram for the 3rd order term corresponding to 3-phonon interaction can be shown as (Mingo (2006)),

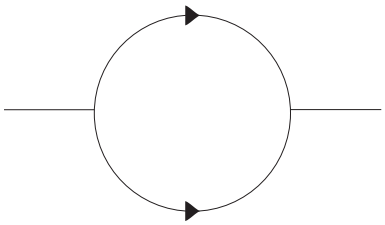

the terms occur from diagrams can be evaluated by following some set of rules given by Wang et al. (Wang et al. (2007)). According to these rules, labeling the left vertex as T_{j_1,j_3,j_5}, and right vertex as T_{j_2,j_4,j_6} where the lines connected to a vertex are labeled as (τ_i, j_i), the diagram corresponds to the term below,

$$\frac{i}{\hbar}\Sigma_{j_1,j_2}(\tau_1,\tau_2) = \sum_{j_3,j_4,j_5,j_6}\int \mathrm{d}\tau_3\mathrm{d}\tau_4\mathrm{d}\tau_5\mathrm{d}\tau_6\ \mathrm{T}_{j_1,j_3,j_5}(\tau_1,\tau_3,\tau_5)\mathrm{T}_{j_2,j_4,j_6}(\tau_2,\tau_4,\tau_6) \times\ G_{j_3,j_4}(\tau_3,\tau_4)G_{j_5,j_6}(\tau_5,\tau_6) \tag{2.150}$$

where G is the linear self-energy without non-linear interactions. At each vertex, the contour times should be equal and we have two delta functions,

$$\begin{aligned}\frac{i}{\hbar}\Sigma_{j_1,j_2}(\tau_1,\tau_2) &= \sum_{j_3,j_4,j_5,j_6}\int \mathrm{d}\tau_3\mathrm{d}\tau_4\mathrm{d}\tau_5\mathrm{d}\tau_6\ \delta(\tau_1-\tau_3)\delta(\tau_3-\tau_5)\mathrm{T}_{j_1,j_3,j_5}(\tau_1,\tau_3,\tau_5) \\ &\quad\times\ \delta(\tau_2-\tau_4)\delta(\tau_4-\tau_6)\mathrm{T}_{j_2,j_4,j_6}(\tau_2,\tau_4,\tau_6) \\ &\quad\times\ G_{j_3,j_4}(\tau_3,\tau_4)G_{j_5,j_6}(\tau_5,\tau_6) \qquad (2.151)\\ &= \sum_{j_3,j_4,j_5,j_6}\mathrm{T}_{j_1,j_3,j_5}\mathrm{T}_{j_2,j_4,j_6}G_{j_3,j_4}(\tau_1,\tau_2)G_{j_5,j_6}(\tau_1,\tau_2) \qquad (2.152)\end{aligned}$$

To obtain the lesser part of this self-energy, we need to convert to real time with branch index $\tau \to t^\sigma$, and this indices are transferred to the Green function,

$$\frac{i}{\hbar}\Sigma^{\sigma_1,\sigma_2}(t_1-t_2) = \sum_{j_3,j_4,j_5,j_6}\mathrm{T}_{j_1,j_3,j_5}\mathrm{T}_{j_2,j_4,j_6}G^{\sigma_1,\sigma_2}_{j_3,j_4}(t_1-t_2)G^{\sigma_1,\sigma_2}_{j_5,j_6}(t_1-t_2) \tag{2.153}$$

The lesser self-energy can be represented as $\Sigma^{+-}(t-t')$ where t is on the upper branch, and t' is on the lower branch,

$$\frac{i}{\hbar}\Sigma^{<}(t_1-t_2) = \sum_{j_3,j_4,j_5,j_6}\mathrm{T}_{j_1,j_3,j_5}\mathrm{T}_{j_2,j_4,j_6}G^{<}_{j_3,j_4}(t_1-t_2)G^{<}_{j_5,j_6}(t_1-t_2) \tag{2.154}$$

We need to use Fourier transform to express this self energy in frequency space,

$$\begin{aligned}\frac{i}{\hbar}\Sigma^{<}(t_1-t_2) &= \sum_{j_3,j_4,j_5,j_6}\int\frac{\mathrm{d}\omega_1}{2\pi}\int\frac{\mathrm{d}\omega_2}{2\pi}\mathrm{T}_{j_1,j_3,j_5}\mathrm{T}_{j_2,j_4,j_6} \\ &\quad\times G^{<}_{j_3,j_4}(\omega_1)G^{<}_{j_5,j_6}(\omega_2)\exp(-i(\omega_1+\omega_2)t) \qquad (2.155)\\ &= \int\Sigma^{<}_{j_1,j_2}(\omega)\frac{\mathrm{d}\omega}{2\pi}\exp(-i\omega t) \qquad (2.156)\end{aligned}$$

Since all integrations are on $(-\infty, \infty)$, by letting $\omega = \omega_1 + \omega_2$, we can express the self-energy as,

$$\int \Sigma^{<}_{j_1,j_2}(\omega)\frac{\mathrm{d}\omega}{2\pi}\exp(-i\omega t) = \int \Sigma^{<}_{j_1,j_2}(\omega)\exp(-i\omega t)\frac{\mathrm{d}\omega_1}{2\pi} + \int \Sigma^{<}_{j_1,j_2}(\omega)\exp(-i\omega t)\frac{\mathrm{d}\omega_2}{2\pi} \tag{2.157}$$

each term has equal contribution since the integral is over all frequencies. Then the first term in the integration can be defined by,

$$\frac{i}{\hbar}\int \Sigma^{<}_{j_1,j_2}(\omega)\exp(-i\omega t)\frac{\mathrm{d}\omega_1}{2\pi} = \frac{1}{2}\sum_{j_3,j_4,j_5,j_6}\int\frac{\mathrm{d}\omega_1}{2\pi}\int\frac{\mathrm{d}\omega_2}{2\pi}\mathrm{T}_{j_1,j_3,j_5}\mathrm{T}_{j_2,j_4,j_6} \times G^{<}_{j_3,j_4}(\omega_1)G^{<}_{j_5,j_6}(\omega_2)\exp(-i\omega t) \tag{2.158}$$

Hence,

$$\frac{i}{\hbar}\Sigma^{<}_{j_1,j_2}(\omega) = \sum_{j_3,j_4,j_5,j_6}\int\frac{\mathrm{d}\omega_2}{4\pi}\mathrm{T}_{j_1,j_3,j_5}\mathrm{T}_{j_2,j_4,j_6}G^{<}_{j_3,j_4}(\omega-\omega_2)G^{<}_{j_5,j_6}(\omega_2) \tag{2.159}$$

the same result is shown by Mingo (2006) with a factor 4π.

the greater self-energy is related to the lesser self-energy with a relation given in Section 2.2.1,

$$\Sigma^{<}(t-t') = \Sigma^{>}(t'-t) \tag{2.160}$$

if we choose t' as zero and take the Fourier transform,

$$\int_{-\infty}^{\infty}\frac{\mathrm{d}\omega}{2\pi}\Sigma^{<}(\omega)\exp(-i\omega t) = \int_{-\infty}^{\infty}\frac{\mathrm{d}\omega}{2\pi}\Sigma^{>}(\omega)\exp(i\omega t) \tag{2.161}$$

by changing the variable from ω to $-\omega$ in the right-hand side and putting a minus sign to preserve limits gives,

$$\int_{-\infty}^{\infty}\frac{\mathrm{d}\omega}{2\pi}\Sigma^{<}(\omega)\exp(-i\omega t) = \int_{-\infty}^{\infty}\frac{\mathrm{d}\omega}{2\pi}\Sigma^{>}(-\omega)\exp(-i\omega t) \tag{2.162}$$

hence,

$$\Sigma^{<}(\omega) = \Sigma^{>}(-\omega) \tag{2.163}$$

now, we can compute the imaginary part of the retarded self-energy,

$$\mathrm{Im}\{\Sigma^{r}(\omega)\} = \frac{1}{2}[\Sigma^{r}(\omega) - \Sigma^{a}(\omega)] \tag{2.164}$$

$$= \frac{1}{2}[\Sigma^{>}(\omega) - \Sigma^{<}(\omega)] \tag{2.165}$$

The real and imaginary parts of a retarded Green function are related to each other with so-called Hilbert transform,

$$\mathrm{Re}\{\Sigma^r(\omega)\} = \mathcal{H}\{\mathrm{Im}\{\Sigma^r(\omega)\}\} \tag{2.166}$$

2.3.2. Mean-Field Approach

In some quantum-mechanical problems, it is hard to tackle with the computational complexities of many-body interactions, and one may perform a mean-field calculation by approximating the interaction as one-body interaction. One such example is the Hartree approximation, where a many-electron wavefunction is approximated by a multiplication of one-electron wavefunctions (Torres (2013)).

Recently, it was shown by Zhang et al. (2013) that the quantum self-consistent mean-field (QSCMF) model for quartic anharmonicity is very accurate in comparison with quantum master equation for systems with weak system-bath coupling. They also showed that nonlinearity enhances thermal transport at the interface of their one-dimensional model with two-atoms. In QSCMF model, the effective dynamical matrix is given by,

$$\widetilde{K}_{ij} = K_{ij} + 6i\hbar \sum_{kl} T_{ijkl} \int_0^\infty \frac{\mathrm{d}\omega}{2\pi} G^<_{kl}(\omega) \tag{2.167}$$

Since $G^<(\omega)$ depends on $G^r(\omega)$ which also depends on $\widetilde{K}$, a self-consistent calculation is required.

2.3.3. Anharmonic Force Constants in 1D

In 1-dimensions, the potential energy can be expanded for a finite chain with each bond having a force constant K,

$$K\sum_{n=1}^{N-1}(\hat{u}_n - \hat{u}_{n+1})^2 = K\sum_{n=1}^{N-1}(\hat{u}_n^2 + \hat{u}_{n+1}^2 - \hat{u}_n\hat{u}_{n+1} - \hat{u}_{n+1}\hat{u}_n) \tag{2.168}$$

Then we can write harmonic force constants $T_{ij} = \frac{1}{2}\left.\frac{\partial^2 V}{\partial u_i \partial u_j}\right|_{u_i=u_j=0}$ as,

$$T_{ij} = \begin{cases} K & , \quad i=j=1 \quad \text{or} \quad i=j=N \\ 2K & , \quad i=j \quad \text{and} \quad 1<i<N \\ -K & , \quad i=j\pm 1 \\ 0 & , \quad \text{otherwise} \end{cases} \tag{2.169}$$

The 3rd order term,

$$K_3 \sum_{n=1}^{N-1} (\hat{u}_n - \hat{u}_{n+1})^3 = K_3 \sum_{n=1}^{N-1} (\hat{u}_n^3 + \hat{u}_n \hat{u}_{n+1}^2 - \hat{u}_n^2 \hat{u}_{n+1} - \hat{u}_n \hat{u}_{n+1} \hat{u}_n - \hat{u}_{n+1} \hat{u}_n^2 - \hat{u}_{n+1}^3 + \hat{u}_{n+1} \hat{u}_n \hat{u}_{n+1} + \hat{u}_{n+1}^2 \hat{u}_n) \tag{2.170}$$

and the force constants $T_{ijk} = \frac{1}{3!} \left. \frac{\partial^3 V}{\partial u_i \partial u_j \partial u_k} \right|_{u_i = u_j = u_k = 0}$ are,

$$T_{ijk} = \begin{cases} K_3 & , \quad i = j = k = 1 \quad \text{or} \quad i = j = k = N \\ K_3 & , \quad i + 1 = j = k \quad \text{or} \quad i = j + 1 = k \\ & \quad \text{or} \quad i = j = k + 1 \\ -K_3 & , \quad i - 1 = j = k \quad \text{or} \quad i = j - 1 = k \\ & \quad \text{or} \quad i = j = k - 1 \\ 0 & , \quad \text{otherwise} \end{cases} \tag{2.171}$$

The 4th order term,

$$\begin{aligned} K_4 \sum_{n=1}^{N-1} (\hat{u}_n - \hat{u}_{n+1})^4 = K_4 \sum_{n=1}^{N-1} (& \hat{u}_n^4 - \hat{u}_n^3 \hat{u}_{n+1} - \hat{u}_n^2 \hat{u}_{n+1} \hat{u}_n \\ & + \hat{u}_n^2 \hat{u}_{n+1}^2 - \hat{u}_n \hat{u}_{n+1} \hat{u}_n^2 + \hat{u}_n \hat{u}_{n+1} \hat{u}_n \hat{u}_{n+1} \\ & + \hat{u}_{n+1} \hat{u}_n^2 \hat{u}_{n+1} - \hat{u}_n \hat{u}_{n+1}^3 - \hat{u}_{n+1} \hat{u}_n^3 \\ & + \hat{u}_{n+1} \hat{u}_n^2 \hat{u}_{n+1} + \hat{u}_{n+1} \hat{u}_n \hat{u}_{n+1} \hat{u}_n - \hat{u}_{n+1} \hat{u}_n \hat{u}_{n+1}^2 \\ & + \hat{u}_{n+1} \hat{u}_n^2 - \hat{u}_{n+1}^2 \hat{u}_n \hat{u}_{n+1} - \hat{u}_{n+1}^3 \hat{u}_n + \hat{u}_{n+1}^4) \end{aligned} \tag{2.172}$$

and $T_{ijkl} = \frac{1}{4!} \left. \frac{\partial^4 V}{\partial u_i \partial u_j \partial u_k \partial u_l} \right|_{u_i = u_j = u_k = u_l = 0}$ are,

$$T_{ijkl} = \begin{cases} K_4 & , \quad i = j = k = 1 \quad \text{or} \quad i = j = k = N \\ 2K_4 & , \quad i = j = k \quad \text{and} \quad i \neq 1 \quad \text{and} \quad i \neq N \\ -K_4 & , \quad i \pm 1 = j = k = l \quad \text{or} \quad i = j \pm 1 = k = l \\ & \quad \text{or} \quad i = j = k \pm 1 = l \quad \text{or} \quad i = j = k = l \pm 1 \\ K_4 & , \quad i = j \quad \text{and} \quad k = l \quad \text{and} \quad j = k \pm 1 \\ & \quad \text{or} \quad i = l \quad \text{and} \quad k = j \quad \text{and} \quad i = j \pm 1 \\ & \quad \text{or} \quad i = k \quad \text{and} \quad l = j \quad \text{and} \quad i = j \pm 1 \\ 0 & , \quad \text{otherwise} \end{cases} \tag{2.173}$$

CHAPTER 3

NUMERICAL CALCULATIONS AND RESULTS

3.1. Software Used for Numerical Calculations

Our transport calculations were performed by using MATLAB (2018). VASP software package (Kresse and Hafner (1993, 1994); Kresse and Furthmüller (1996); Kresse and Furthmüller (1996)) were used to perform DFT calculations with projector augmented wave (PAW) method (Blöchl (1994); Kresse and Joubert (1999)) with generalized gradient approximation (GGA) (Perdew et al. (1992, 1993)). SciPy (Jones et al. (01)) library is used to analyse our DFT results, and Matplotlib (Hunter (2007)) library is used to visualize the results.

3.2. Carbon Chain Force Constants

For a one-dimensional carbon chain, VASP DFT calculation is performed for 2 atoms per unit cell with 600 eV plane wave cutoff, projector augmented wave method with generalized gradient approximation pseudopotentials, and Brilloin zone is sampled with 9 points. The calculation is performed for varying C-C bond lengths between 1.0 and 3.0 to find minimum energy. This calculation is performed to determine the orders of magnitude of force constants in real crystals.

Figure By using the data from DFT, a 8^{th} order curve fit is performed, and energy as a function of displacement is plotted (Figure 3.1). The y-axis is shifted to zero ($K_0 = 0$). As we can see in Figure 3.1, 2^{nd},3^{rd} and 4^{th} terms are the largest contribution to the potential at the order of a nanometer. The potential due to these terms is given by,

$$V(x) = 8.557 \times 10^1 \, x^4 - 1.678 \times 10^2 \, x^3 + 8.687 \times 10^1 \, x^2 \tag{3.1}$$

where x is the displacement in Å and $[V(x)] = \text{eV}$.

To determine the contribution of each term, their separate plots are given in Figure 3.2. The effect of the 4^{th} order term is almost negligible at very small displacements where harmonic term dominates. Also Figure 3.2 shows that at the order of $0.1 \text{ eV} \approx 10^6 \text{K}$,

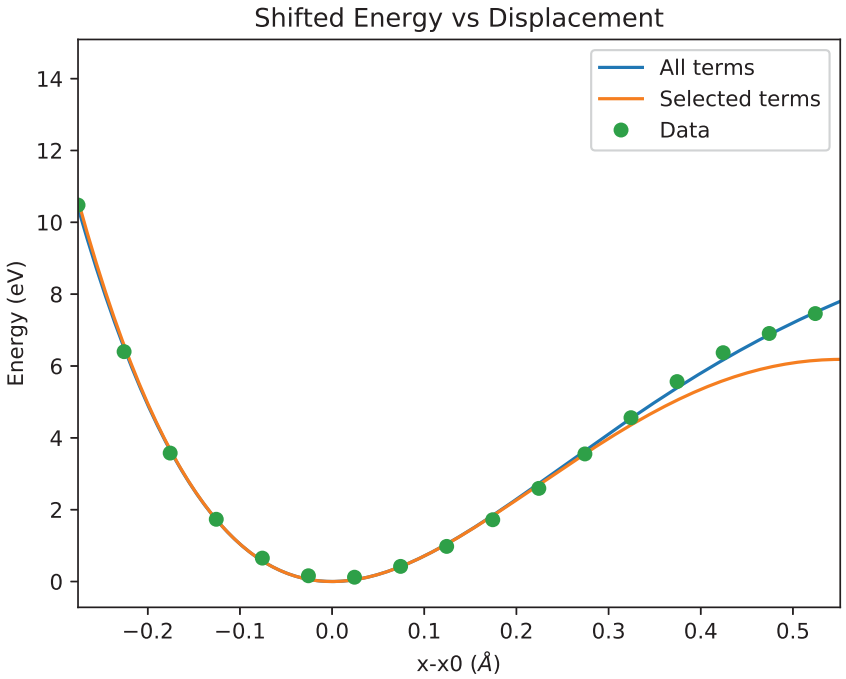

Figure 3.1. Energy vs. displacement for a chain of carbon atoms. All terms of the 8$^{\text{th}}$ order curve fit (blue line), and selected terms corresponding to the 2$^{\text{nd}}$,3$^{\text{rd}}$ and 4$^{\text{th}}$ terms (orange line) and DFT data (green dots) are shown.

$n = 3$ term is significant. At room temperature $300K \approx 0.025$ meV the curve for $n = 3$ becomes as flat as that of $n = 4$, indicating no significance.

To calculate corresponding mass-normalized force constants, we need to consider mass of a carbon = $12.01 \times 1.660 \times 10^{-27}$ kg $= 1.993\,66 \times 10^{-26}$ kg. By using (1.99),

$$V(u) = 4.36 \times 10^{27}\, u^2 - 5.96 \times 10^{40}\, u^3 + 2.153 \times 10^{53}\, u^4 \tag{3.2}$$

3.3. Calculations for the Diagrammatic Technique

The self-energies corresponding to the selected diagrams are computed using a self-consistent procedure. The algorithm includes the following steps;

1. Computation of retarded self-energies of the reservoirs $\Sigma_{\text{L/R}}(\omega)$, broadening functions $\Gamma_{\text{L/R}}(\omega)$ and lesser self-energies of the equilibrium system, $\Sigma^{<}_{\text{L/R}}(\omega)$.

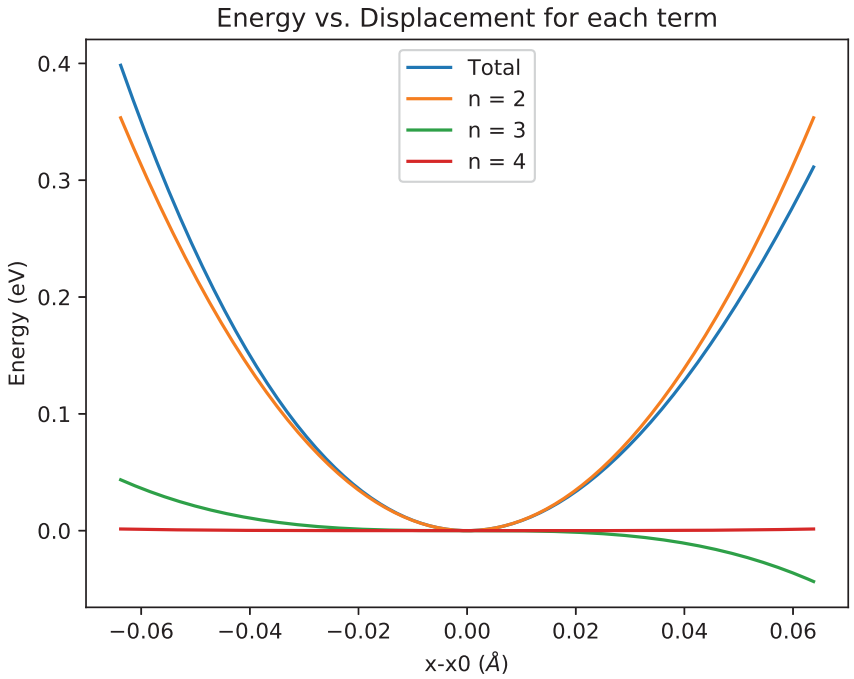

Figure 3.2. Plot of total energy and n^{th} term for n=2,3,4 versus displacement. The most important contribution is from harmonic term. As n increases, the contribution of n^{th} term to the potential decreases.

2. Computation of lesser Green function of the device using the equilibrium lesser self-energy,

$$G_{\mathrm{C}}^{<}(\omega) = \sum_{i\in\{\mathrm{L,R}\}} G_{\mathrm{C}}^{\mathrm{r}}(\omega)\Sigma_{\mathrm{j}}^{<}(\omega)G_{\mathrm{C}}^{\mathrm{a}}(\omega) \tag{3.3}$$

3. With the retarded self energies known, computation of retarded Green function of the device by using (2.76).

4. For each iteration,

   - Computation of the lesser anharmonic self-energy, $\Sigma_{\mathrm{C}}^{<}(\omega)$ by using the lesser and greater Green functions of the device $G_{\mathrm{C}}^{<}(\omega)$.
   - With $\Sigma_{\mathrm{C}}^{<}(\omega) = \Sigma_{\mathrm{C}}^{>}(-\omega)$ is known, by using (2.15) computation of the imaginary part of the retarded anharmonic self-energy $\Sigma_{\mathrm{C}}^{\mathrm{r}}$.
   - Computation of the real part from the imaginary part of the retarded anharmonic self energy via Hilbert transform.

- Computation of the retarded green function of the device with (2.76) by using,

$$\widetilde{K} = K + \Sigma_{\mathrm{L}}^{\mathrm{r}} + \Sigma_{\mathrm{R}}^{\mathrm{r}} + \Sigma_{\mathrm{C}}^{\mathrm{r}} \tag{3.4}$$

- Computation of lesser and greater Green functions by using the definitions (2.135) and (2.136) for equilibrium, with the retarded Green function of the central part.

- Check convergence with the change in total energy

$$\delta E = \frac{E_{n+1} - E_N}{E_{n+1} + E_n} \tag{3.5}$$

5. After the convergence is achieved, compute DOS via (2.44) and transmission coefficient via (2.83) by using self-consistently calculated $G_{\mathrm{C}}^{\mathrm{r}}(\omega)$.

In our calculations, ω is chosen between $-\omega_{\max}$ and $\omega_{\max}$ where $\omega_{\max} > 0$. The reason is that by only calculating lesser or greater Green function on a symmetric mesh, one can determine greater (lesser) Green function from lesser (greater) Green function by using the identity (2.114). η is chosen to be 10^{-8}, harmonic force constant $K = 4.36 \times 10^{27}\mathrm{eV\ \AA^{-2}\ kg^{-1}}$. For the recursive calculation of reservoir Green functions, a cutoff value of 10^{-8} and 1000 maximum iterations are chosen as convergence conditions for the recursive algorithm.

DOS, transmission function and conductance are calculated by using both 3$^{\text{rd}}$ and 4$^{\text{th}}$ order diagrams and QSCMF method for 4$^{\text{th}}$ order term. In conductance calculations, we consider that the system is in thermal equilibrium with the reservoirs.

Figures 3.3,3.4 show how DOS and Transmission functions of two-atom device vary with anharmonic coupling strength at constant temperature for the 3$^{\text{rd}}$ and 4$^{\text{th}}$ order diagrammatic self-energies respectively. The effect of anharmonicity due to the coupling determined from DFT calculation is so small that it is negligible. Increasing anharmonic coupling strength about several orders of magnitude can provide significant results. However, increasing the coupling strength makes it harder to determine convergency in self-consistent calculation. For this reason, we only consider the temperatures up to 1000 Kelvin which is much more greater than the room temperature. As coupling strength increases, the transmission function gets smaller in band edge as a result of scattering of phonons from other phonons which can be seen in the figures.

In section 1.4.2, it is mentioned that MFP for 3-phonon scattering is inversely proportional to the square of the frequency. Currently, our codes are not efficient enough to calculate larger systems to investigate diffusive behavior, however the decay at band

edge (higher frequencies) with increasing anharmonicity indicates that the mean free path is smaller at large frequencies which is consistent with literature.

The results are highly dependent on the frequency mesh, because we perform a numerical integration. Convergence is checked by the difference in total energy between consecutive iterations n and $n+1$ as $\delta_E = (E_{n+1} - E_n)/(E_{n+1} + E_n)$, and a mixing is performed for better convergence. For 3rd order diagram, convergence cutoff for self-consistent iterations is chosen to be 10^{-4} and for 4th order diagram and mean-field calculation it is choosen to be 10^{-8}.

As it is shown in Figure 3.5, if temperature increases the effect of anharmonicity increases. Y-axis is choosen to be [0.99,1] to see the difference clearly. We can determine this behavior from both DOS and Transmission plots in the figure. The effect of the 4th order term is much smaller than the 3rd order term, so we cannot see any variation in DOS and transmission with respect to the temperature as shown in Figure 3.6 for 4th order diagram.

The conductance as a function of temperature for different coupling strengths due to the 3rd and 4th order diagrams are given in Figure 3.7 and Figure 3.8 respectively. Even though phonons which carry heat increase thermal conductance at lower temperatures, at higher temperatures the number of phonons which scatter from each other increases and this cause the suppression of thermal conductance at higher temperatures with respect to the temperature corresponding to a hill in conductance. Our results do not have this behavior in temperatures below 1000 Kelvin for a small system ($\sim$10 atoms), however the suppression in conductance due to anharmonicity can be observed in the figures.

3.4. Mean-Field Calculations

The algorithm for the mean-field calculation is similar, however we modify the dynamical matrix instead of modifying self-energy at each iteration. When it comes to computing retarded Green function, both methods involve an effective dynamical matrix. The effective dynamical matrix is given by (Zhang et al. (2013)),

$$\widetilde{K}_{ij} = K_{ij} + 6i\hbar \sum_{kl} \int_0^\infty \mathrm{d}\omega \; T_{ijkl} G^<_{kl}(\omega) \tag{3.6}$$

The lowest order diagram for the 4th order term is shown as below,

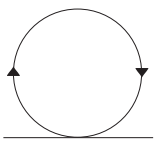

The self energy corresponding to this diagram is given by Mingo (2006),

$$i\Sigma^{\mathrm{r}}_{ij} = \hbar \sum_{kl} \int_{-\infty}^{\infty} \mathrm{d}\omega \; T_{iklj}(G^{<}_{kl}(\omega) + G^{>}_{lk}(\omega)) \tag{3.7}$$

In Figure 3.9 and Figure 3.10, mean-field DOS and transmission values for varying anharmonic coupling and for varying temperature is represented respectively. In comparison with the diagrammatic method in Figure 3.6, the variation in DOS and Transmission with respect to the temperature is smaller. However the the differences are less than 10^{-3}, so the conductance curves are nearly equivalent as it can be seen in Figures 3.8 and 3.11.

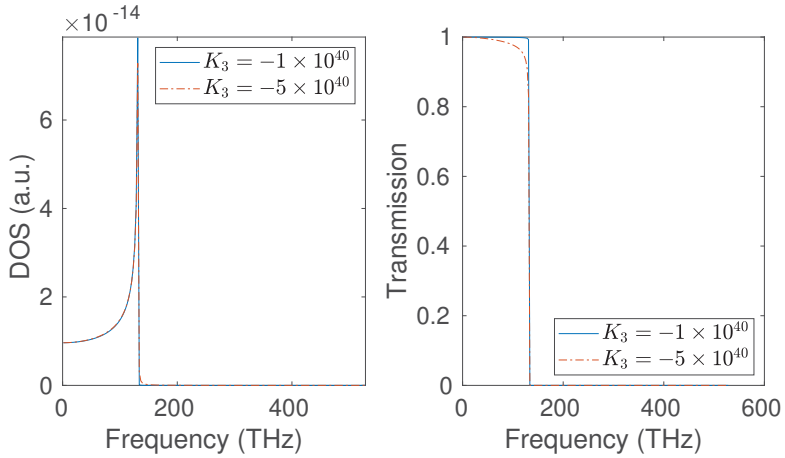

Figure 3.3. Plot of DOS and Transmission function of a two-atom device from a 3rd order diagram with respect to frequency for varying anharmonic coupling strength at $T = 343.3\mathrm{K}$. $\omega_{\max} = 528.2\mathrm{THz}$ sampled with 400 points. The unit of K_3 is $\mathrm{eV\ \AA^{-3}kg^{-3/2}}$.

A comparison of conductance determined by using QSCMF and diagrammatic method is given by Figure 3.13. For temperatures up to 1000 K, as temperature increases the discrepancy in conductance curves obtained by two methods increases. For small coupling in this temperature range, we can observe that the results from both methods are equivalent.

As number of atoms in the device increases, the number of displacements which contribute to anharmonicity increases, so the effect is expected to be stronger. However our results for temperatures up to 1000 K shows in Figure 3.12 that 10-atom anharmonic chain is still a small system to observe such effects with the anharmonic constant at the order of which is determined from DFT.

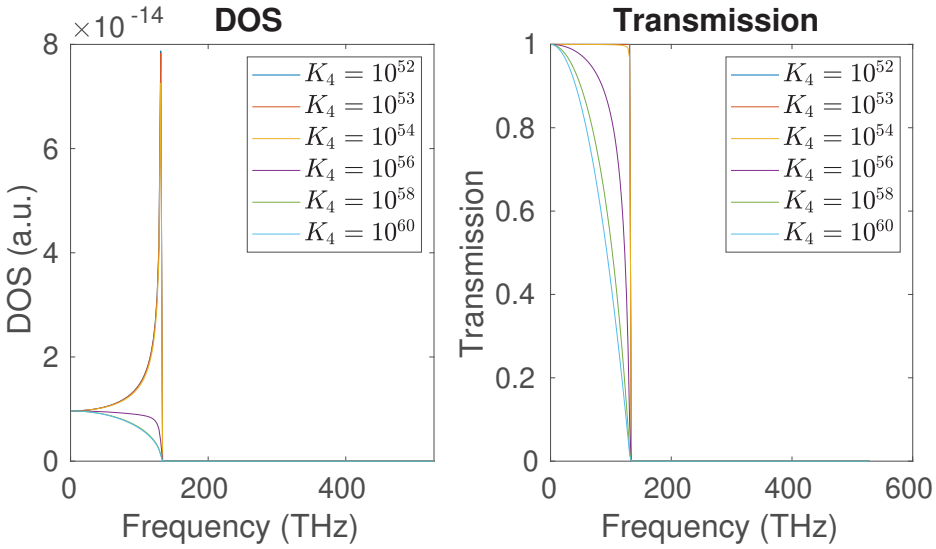

Figure 3.4. Plot of DOS and Transmission function of a two-atom device from a 4th order diagram with respect to frequency for varying anharmonic coupling strength at $T = 343.3\text{K}$. $\omega_{\max} = 528.2\text{THz}$ sampled with 400 points. The unit of K_4 is $\text{eV Å}^{-4}\text{kg}^{-2}$.

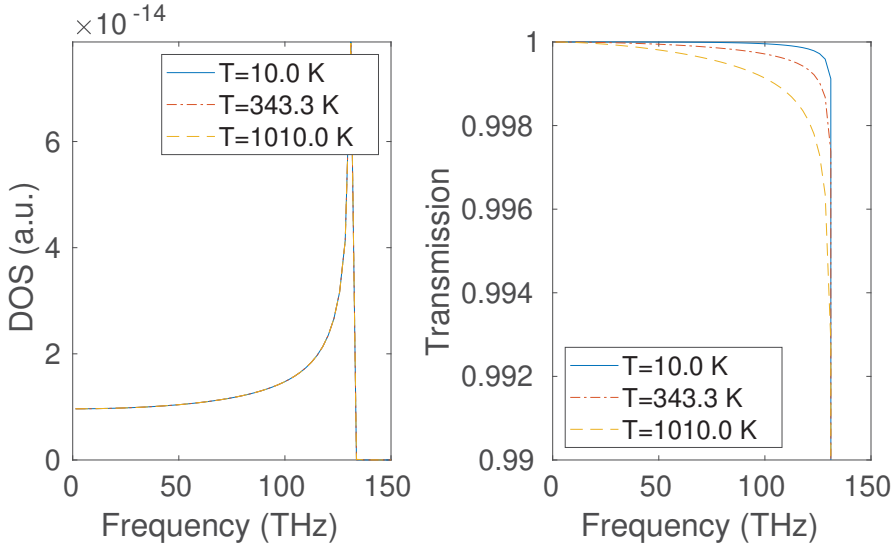

Figure 3.5. Plot of DOS and Transmission function of a two-atom device from a 3rd order diagram with respect to frequency for varying temperature at $K_3 = -10^{40}\text{eV Å}^{-3}\ \text{kg}^{-3/2}$. $\omega_{\max} = 528.2\text{THz}$ sampled with 400 points.

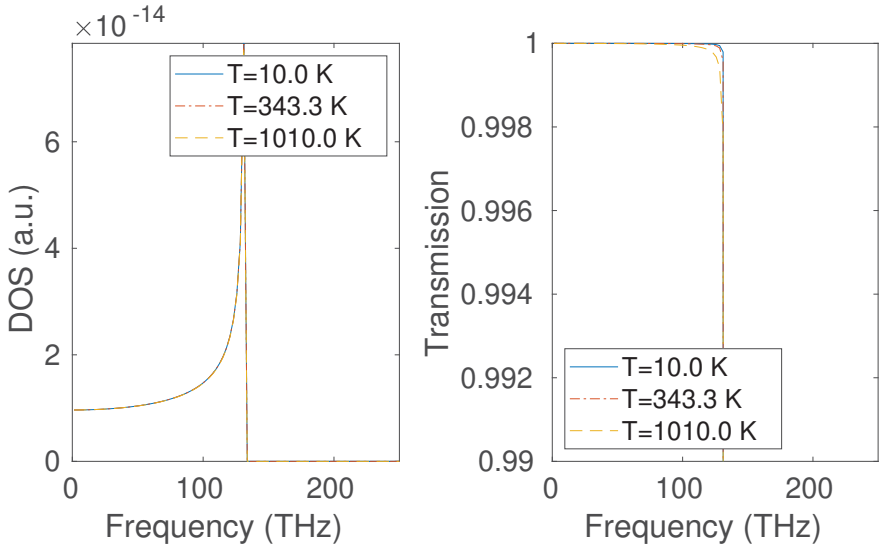

Figure 3.6. Plot of DOS and Transmission function of a two-atom device from a 4th order diagram with respect to frequency for varying temperature at $K_4 = 10^{53}\text{eV Å}^{-4}\,\text{kg}^{-2}$. $\omega_{\max} = 528.2\text{THz}$ sampled with 400 points.

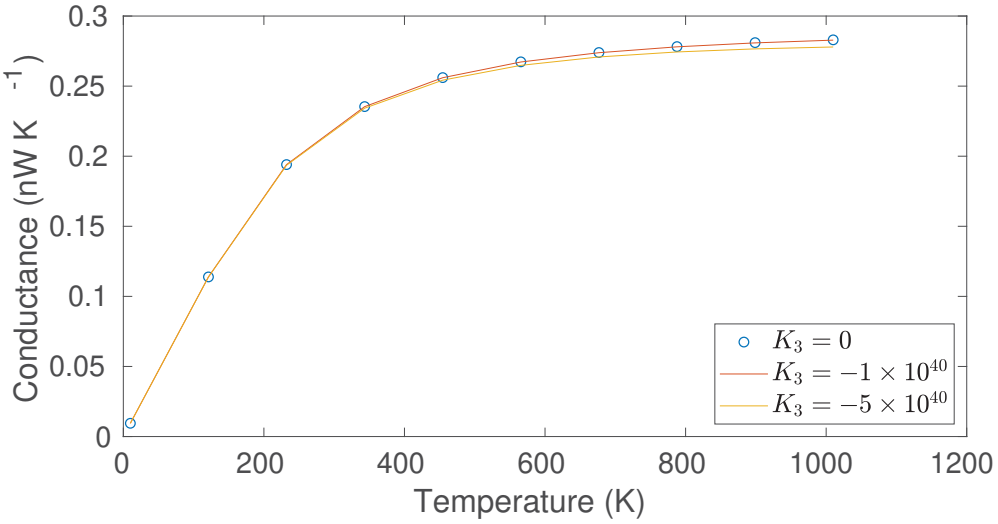

Figure 3.7. Plot of conductance of a two-atom device from a 3rd order diagram as a function of temperature for varying anharmonic coupling. $\omega_{\max} = 528.2\text{THz}$ sampled with 400 points, T is sampled with 10 points between 10 and 1010. The unit of K_3 is $\text{eV Å}^{-3}\text{kg}^{-3/2}$.

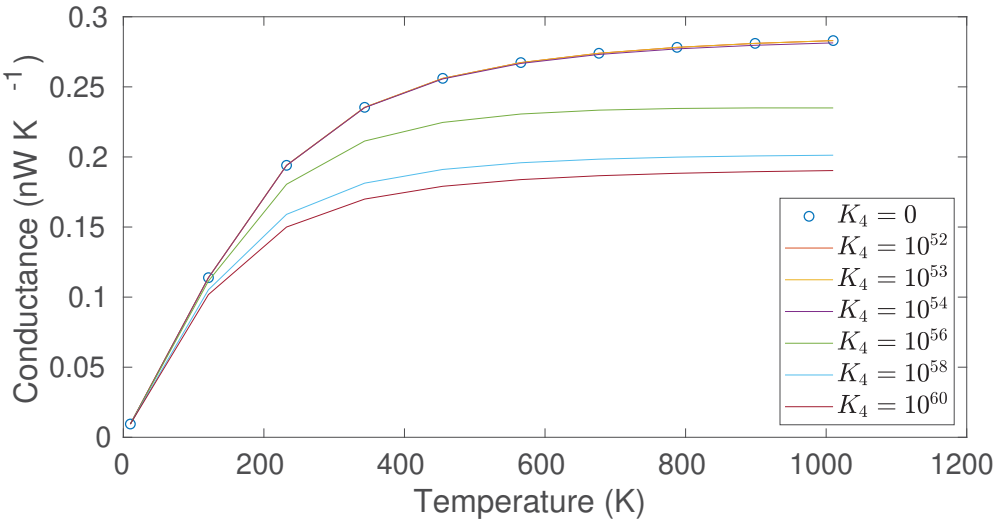

Figure 3.8. Plot of conductance of a two-atom device from a 4th order diagram as a function of temperature for varying anharmonic coupling. $\omega_{\max} = 528.2\text{THz}$ sampled with 400 points, T is sampled with 10 points between 10 and 1010. The unit of K_4 is $\text{eV Å}^{-4}\text{kg}^{-2}$.

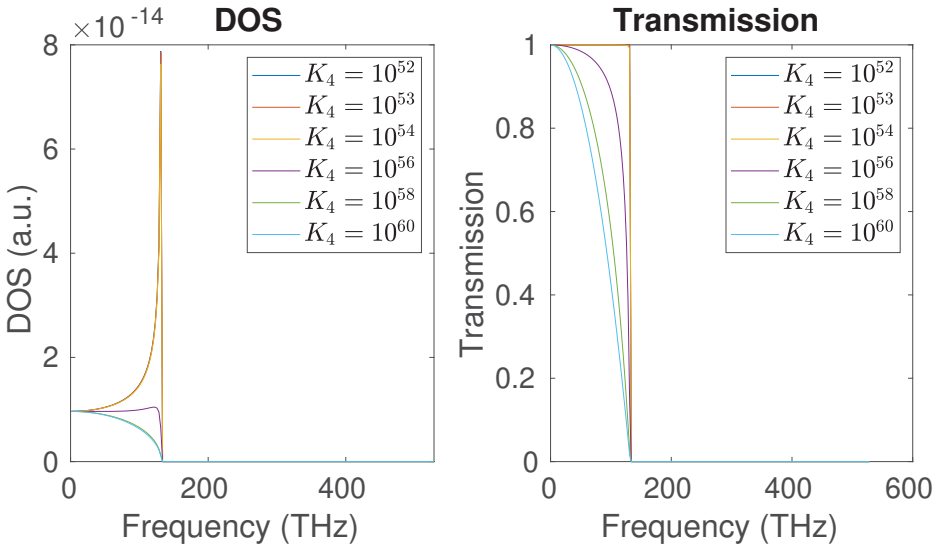

Figure 3.9. Plot of 4th Mean-Field DOS and Transmission function of a two-atom device with respect to frequency for varying anharmonic coupling strength at $T = 343.3\text{K}$. $\omega_{\max} = 528.2\text{THz}$ sampled with 400 points. The unit of K_4 is $\text{eV Å}^{-4}\text{kg}^{-2}$.

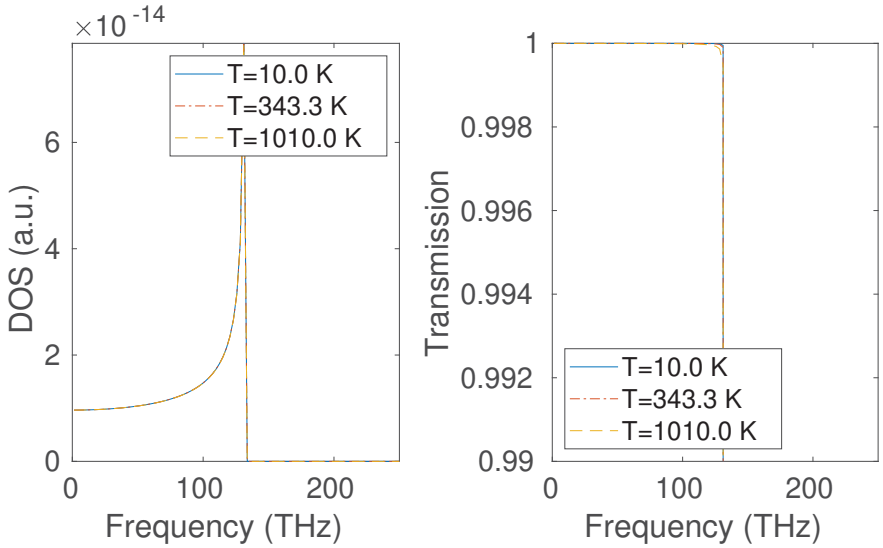

Figure 3.10. Plot of 4th order mean-field DOS and Transmission function of a two-atom device with respect to frequency for varying temperature at $K_4 = 10^{53}\text{eV Å}^{-4}\,\text{kg}^{-2}$. $\omega_{\max} = 528.2\text{THz}$ sampled with 400 points.

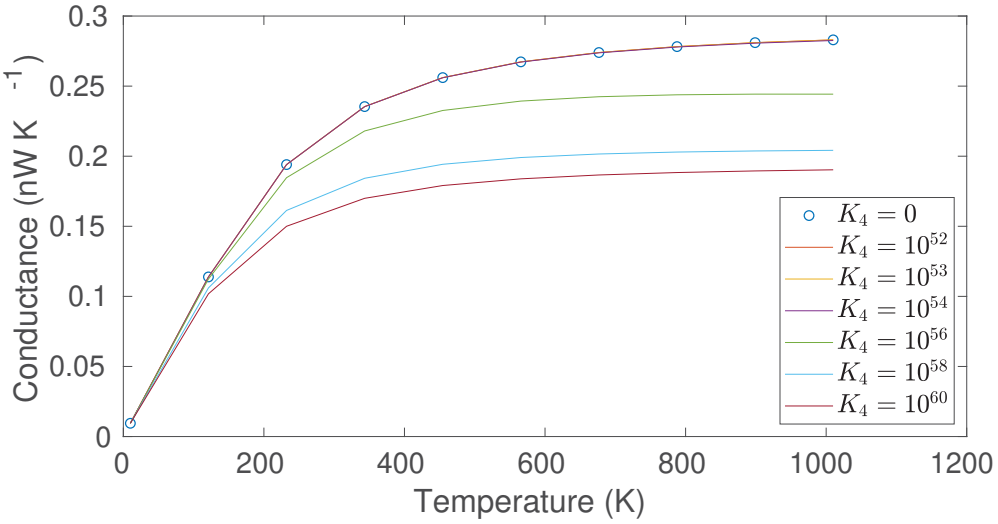

Figure 3.11. Plot of 4th mean-field conductance as a function of temperature for varying anharmonic coupling. $\omega_{\max} = 528.2\text{THz}$ sampled with 400 points, T is sampled with 10 points between 10 and 1010. The unit of K_4 is $\text{eV Å}^{-4}\text{kg}^{-2}$.

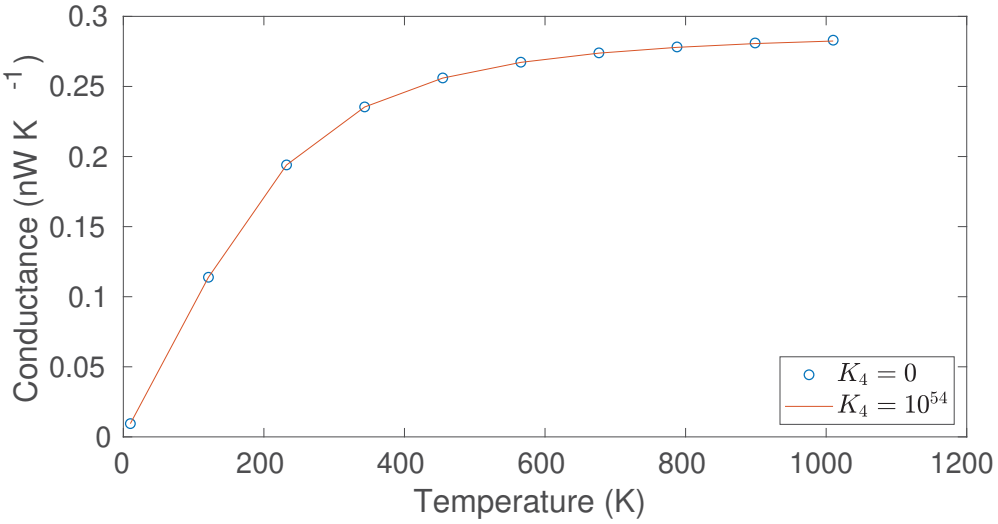

Figure 3.12. 4th order mean-field conductance plot of a 10-atom device for $K_4 = 10^{54}\text{eV Å}^{-4}\,\text{kg}^{-2}$. $\omega_{\max} = 528.2\text{THz}$ sampled with 400 points, and T is sampled with 10 points between 10 and 1010.

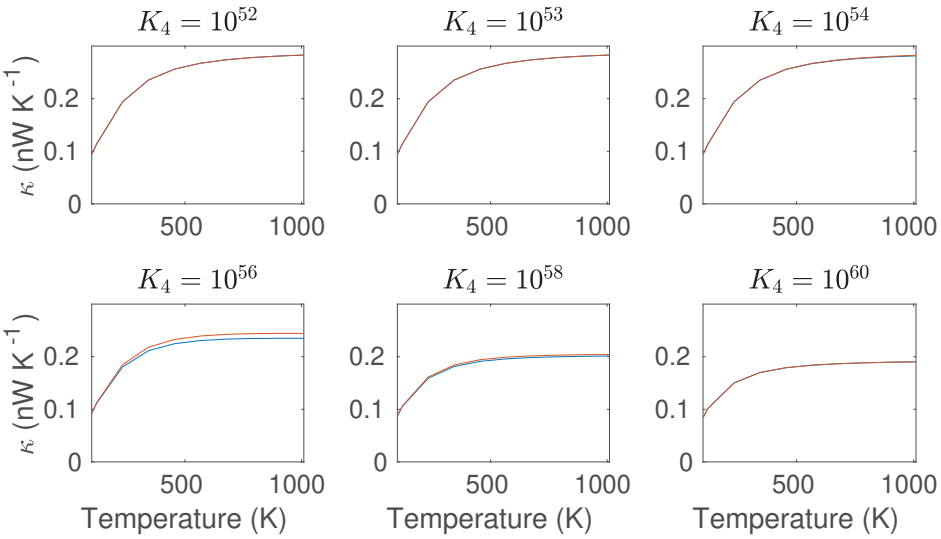

Figure 3.13. Comparison of conductance curves determined by diagrammatic method and QSCMF for different coupling strength as a function of temperature. Blue curve corresponds to diagrammatic method, while red curve corresponds to QSCMF method. $\omega_{\max} = 528.2\text{THz}$ sampled with 400 points, and T is sampled with 10 points between 10 and 1010. The unit of K_4 is $\text{eV Å}^{-4}\text{kg}^{-2}$

CHAPTER 4

CONCLUSION

In this study, we investigate anharmonicity using NEGF method in one-dimensional monoatomic chains. Anharmonic force constants are determined from DFT calculation of energy for a monoatomic chain of carbon atoms which is performed for varying bond lengths. By curve-fitting this data, we obtain higher order terms in energy as a polynomial function of displacement the coefficients of which can be used to compute transport properties.

In real crystals there are very large numbers of atoms corresponding to very large number of displacements interacting with each other. This cause a suppression in thermal conductance. By increasing the number of atoms to 10, we cannot see a significant difference in conductance for temperatures less than 1000 K (Figure 3.12).

The suppression of conductance also depends on the temperature, and can be seen more clearly in Figure 3.7. It indicates that as temperature increases the suppression effect increases, which is the expected behavior in real systems. The reason is that temperature is related to the number of phonons, as the number of phonons increase, the probability that a phonon interact with another phonon increases, hence conductance decreases. As mentioned in 1.4.2, MFP due to the 3$^{\mathrm{rd}}$ order term is proportional to the ω^{-2}. Our results show that at higher frequencies MFP is smaller and this is consistent with the literature.

Because of the high computational cost in diagrammatic method, one may adopt a mean-field theoretical model (QSCMF) which is computationally more feasible than diagrammatic method, since in diagrammatic method one must take multiple diagrams into account, though we considered only the diagram corresponding to the lowest order self-energy. However, as it is pointed out before, convergence may not be achieved easily for strong coupling and/or very high temperature, and it should be checked for consistency. To check convergency, we can calculate the differences in total energy which is related to DOS as the imaginary part of the Green function for each consecutive iteration. Because the real and the imaginary parts of the Green function are dependent on each other via Hilbert transformation, convergent imaginary (or real) part leads to a convergent Green function. A mixing between consecutive iterations may lead convergence in some cases where the system gets stuck between two saddle points without converging.

The next step for this study is to derive expressions for other anharmonic terms

to perform a similar self-consistent calculation. Further, some numerical tricks should be considered for calculation of effective dynamical matrix. For example, if force constants are stored in a multi-dimensional array a large number of unnecessary multiplication with zeros will be performed due to (3.6). Instead, the equations corresponding to nonzero multiplications in summation may be hardcoded into a for loop to make the calculation much faster than before, making calculations for larger systems possible. Also, it is possible for this model to predict a larger system by observing how self-energy or effective dynamical matrix elements of a smaller convergent system vary spatially.

REFERENCES

Blöchl, P. E. (1994, Dec). Projector augmented-wave method. *Phys. Rev. B 50*, 17953–17979.

Brau, C. A. (2003). *Modern Problems in Classical Electrodynamics (Physics)*. Oxford University Press.

Buot, F. (2009). *Nonequilibrium quantum transport physics in nanosystems : foundation of computational nonequilibrium physics in nanoscience and nanotechnology*. Singapore Hackensack, N.J: World Scientific Pub. Co.

Cahill, D. G., P. V. Braun, G. Chen, D. R. Clarke, S. Fan, K. E. Goodson, P. Keblinski, W. P. King, G. D. Mahan, A. Majumdar, H. J. Maris, S. R. Phillpot, E. Pop, and L. Shi (2014, mar). Nanoscale thermal transport. II. 2003–2012. *Applied Physics Reviews 1*(1), 011305.

Cahill, D. G., W. K. Ford, K. E. Goodson, G. D. Mahan, A. Majumdar, H. J. Maris, R. Merlin, and S. R. Phillpot (2003, jan). Nanoscale thermal transport. *Journal of Applied Physics 93*(2), 793–818.

Chen, G. (2000, apr). Phonon heat conduction in nanostructures. *International Journal of Thermal Sciences 39*(4), 471–480.

Datta, S. (1995). *Electronic Transport in Mesoscopic Systems*. Cambridge University Press.

Devreese, J. T. (1976). *Linear and Nonlinear Electron Transport in Solids*. Boston, MA: Springer US Imprint Springer.

Fowler (1967). *Statistical Mechanics: The theory of the properties of matter in equilibrium, 2nd edition*. Cambridge University Press.

Haug, H. and A.-P. Jauho (2007). *Quantum Kinetics in Transport and Optics of Semiconductors (Springer Series in Solid-State Sciences)*. Springer.

Hirose, K. and N. Kobayashi (2014). *Quantum Transport Calculations for Nanosystems*. Pan Stanford.

Hofmann, P. (2015). *Solid State Physics: An Introduction*. Wiley-VCH.

Hopkins, P. E. and J. R. Serrano (2009, nov). Phonon localization and thermal rectification in asymmetric harmonic chains using a nonequilibrium green's function formalism. *Physical Review B 80*(20).

Hunter, J. D. (2007). Matplotlib: A 2d graphics environment. *Computing In Science & Engineering 9*(3), 90–95.

Jones, E., T. Oliphant, P. Peterson, et al. (2001–). SciPy: Open source scientific tools for Python. [Online; accessed August 8, 2018].

Kittel, C. (2005). *Introduction to solid state physics*. Hoboken, NJ: Wiley.

Kittel, C. and P. B. Kahn (1965, jun). Quantum theory of solids. *American Journal of Physics 33*(6), 517–518.

Kresse, G. and J. Furthmüller (1996, jul). Efficiency of ab-initio total energy calculations for metals and semiconductors using a plane-wave basis set. *Computational Materials Science 6*(1), 15–50.

Kresse, G. and J. Furthmüller (1996, Oct). Efficient iterative schemes for ab initio total-energy calculations using a plane-wave basis set. *Phys. Rev. B 54*, 11169–11186.

Kresse, G. and J. Hafner (1993, Jan). Ab initio molecular dynamics for liquid metals. *Phys. Rev. B 47*, 558–561.

Kresse, G. and J. Hafner (1994, May). Ab initio molecular-dynamics simulation of the liquid-metal–amorphous-semiconductor transition in germanium. *Phys. Rev. B 49*, 14251–14269.

Kresse, G. and D. Joubert (1999, Jan). From ultrasoft pseudopotentials to the projector augmented-wave method. *Phys. Rev. B 59*, 1758–1775.

Liu, Y.-W. (2012). Hilbert transform and applications. In S. Salih (Ed.), *Fourier Transform*, Chapter 12. Rijeka: InTech.

Mahan, G. D. (2000). *Many-Particle Physics*. Springer US.

Mahan, G. D. (2010). *Condensed Matter in a Nutshell*. Princeton University Press.

MATLAB (2018). *R2018a*. Natick, Massachusetts: The MathWorks Inc.

Mendoza, J. and G. Chen (2016, dec). Anderson localization of thermal phonons leads to a thermal conductivity maximum. *Nano Letters 16*(12), 7616–7620.

Mingo, N. (2006, sep). Anharmonic phonon flow through molecular-sized junctions. *Physical Review B 74*(12).

Müller, W., R. Schiller, and W. Nolting (2000, aug). Understanding of surface states in a correlated electron system. *The European Physical Journal B 16*(4), 705–718.

Ohno, K. (1999). *Computational Materials Science : From Ab Initio to Monte Carlo Methods*. Berlin, Heidelberg: Springer Berlin Heidelberg.

Perdew, J. P., J. A. Chevary, S. H. Vosko, K. A. Jackson, M. R. Pederson, D. J. Singh, and C. Fiolhais (1992, Sep). Atoms, molecules, solids, and surfaces: Applications of the generalized gradient approximation for exchange and correlation. *Phys. Rev. B 46*, 6671–6687.

Perdew, J. P., J. A. Chevary, S. H. Vosko, K. A. Jackson, M. R. Pederson, D. J. Singh, and C. Fiolhais (1993, Aug). Erratum: Atoms, molecules, solids, and surfaces: Applications of the generalized gradient approximation for exchange and correlation. *Phys. Rev. B 48*, 4978–4978.

Ryndyk, D. (2016). *Theory of Quantum Transport at Nanoscale: An Introduction (Springer Series in Solid-State Sciences)*. Springer.

Sakurai, J. J. and J. J. Napolitano (2010). *Modern Quantum Mechanics (2nd Edition)*. Pearson.

Sancho, M. P. L., J. M. L. Sancho, J. M. L. Sancho, and J. Rubio (1985, apr). Highly convergent schemes for the calculation of bulk and surface green functions. *Journal of Physics F: Metal Physics 15*(4), 851–858.

Simon R. Phillpot, A. J. H. M. (2005). Introduction to thermal transport. *Materials Today 8*(6), 18–20.

Srivastava, G. (1990). *The Physics of Phonons*. CRC Press.

Srivastava, G. (2006). Lattice Thermal Conduction Mechanism in Solids. In S. L. Shindé and J. S. Goela (Eds.), *High Thermal Conductivity Materials*, pp. 1–35. New York, NY: Springer New York.

Stefanucci, G. and R. van Leeuwen (2013). *Nonequilibrium Many-Body Theory of Quantum Systems: A Modern Introduction*. Cambridge University Press.

Torres, L. E. F. F. (2013). *Introduction to Graphene-Based Nanomaterials: From Electronic Structure to Quantum Transport*. Cambridge University Press.

Wang, J.-S., B. K. Agarwalla, H. Li, and J. Thingna (2013, may). Nonequilibrium green's function method for quantum thermal transport. *Frontiers of Physics 9*(6), 673–697.

Wang, J.-S., N. Zeng, J. Wang, and C. K. Gan (2007, jun). Nonequilibrium green's function method for thermal transport in junctions. *Physical Review E 75*(6).

Zhang, G. (2015). *Nanoscale Energy Transport and Harvesting : A Computational Study*. Boca Raton, FL: Pan Stanford Publishing.

Zhang, L., J. Thingna, D. He, J.-S. Wang, and B. Li (2013). Nonlinearity enhanced interfacial thermal conductance and rectification. *EPL (Europhysics Letters) 103*(6), 64002.

Zhou, H., G. Zhang, J.-S. Wang, and Y.-W. Zhang (2016, nov). Phonon transport in a one-dimensional harmonic chain with long-range interaction and mass disorder. *Physical Review E 94*(5).

Zhu, Y., L. Liu, and H. Guo (2016). *Atomistic Simulation of Quantum Transport in Na-*

noelectronic Devices:(With CD-ROM). World Scientific Publishing Co.

Ziman, J. (2001). *Electrons and Phonons*. Oxford University Press.

Ziman, J. M. (1972). *Principles of the Theory of Solids* (2 ed.). Cambridge University Press.

APPENDIX A

NUMBERICAL HILBERT TRANSFORMATION

Given that a complex valued function $H(s)$ is analytic in the entire right half-plane, Kramers-Krönig relations describes the relation between real and imaginary parts of the function (Liu (2012)),

$$H_I(\omega) = \frac{1}{\pi}\int_{-\infty}^{\infty}\frac{H_R(u)\mathrm{d}u}{\omega - u} \tag{A.1}$$

$$H_R(\omega) = -\frac{1}{\pi}\int_{-\infty}^{\infty}\frac{H_I(u)\mathrm{d}u}{\omega - u} \tag{A.2}$$

and Hilbert transform is given by (Liu (2012)),

$$g(x) = \frac{1}{\pi}\int_{-\infty}^{\infty} f(u)\frac{1}{x-u}\mathrm{d}u \tag{A.3}$$

so that,

$$H_I(\omega) = g(H_R(u)) \tag{A.4}$$

$$H_R(\omega) = -g(H_I(u)) \tag{A.5}$$

A physical example to this case is dielectric susceptibility,

$$\chi(\omega) = \epsilon(\omega)/\epsilon_0 - 1 \tag{A.6}$$

Dielectric susceptibility is given by the Fourier transform of a response function (Brau (2003)),

$$\chi(\omega) = \int_{-\infty}^{\infty}\mathrm{G}(\tau)\exp(i\omega\tau)\mathrm{d}\tau \tag{A.7}$$

where $G(\tau)$ is the response function. As an example, we can choose $G(\tau)$ as,

$$G(\tau) = \theta(\tau)\exp(-\alpha\tau) \tag{A.8}$$

such that the response function becomes,

$$\begin{aligned}\chi(\omega) &= \frac{1}{\alpha - i\omega} \\ &= \frac{\alpha}{\alpha^2+\omega^2} + i\frac{\omega}{\alpha^2+\omega^2}\end{aligned} \tag{A.9}$$

Note that $\chi(\omega)$ has a form similar to Equation 2.37. The exact values and Hilbert transformed real and imaginary parts are compared in Figure A.1.

The calculation of susceptibility for Figure A.1 is performed on a 201-point mesh on the interval [-100,100] with $\alpha = 1$.

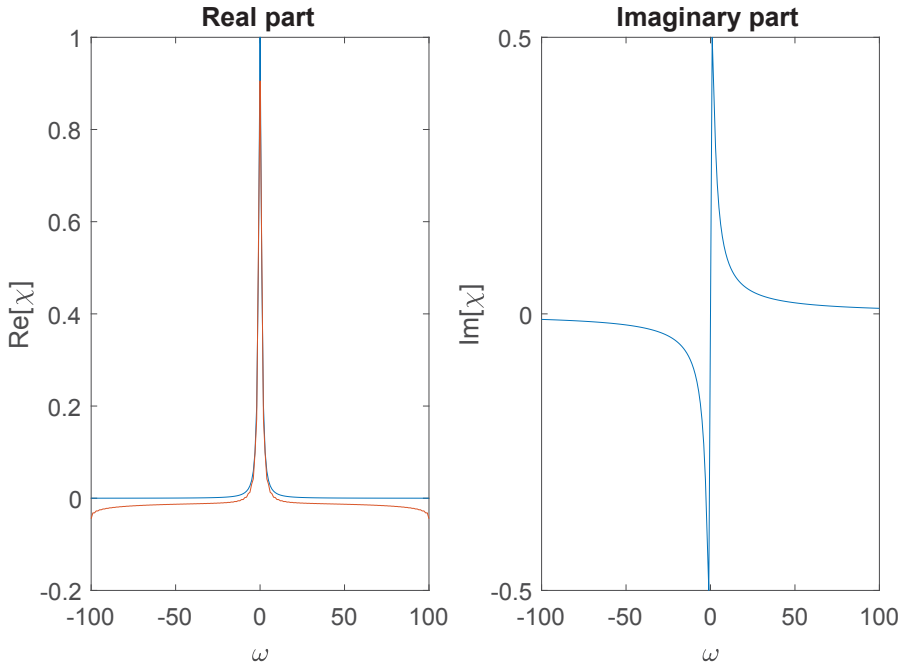

Figure A.1. Negative the Hilbert transform of the imaginary part of the susceptibility (left), and the imaginary part of the susceptibility (right). Blue line shows the exact value while red line represents the Hilbert transform of the imaginary part.